Multi-omics Analysis at Serum Proteomic and Metabolomic Levels Reveals Mechanisms of Moxibustion for a Mouse Model of Ankylosing Spondylitis

Xiao Xu
Zhejiang Chinese Medical University
Ting Liu
Zhejiang Chinese Medical University
Rong-Yun Wang
Zhejiang Chinese Medical University
Ya-Nan Shi
Zhejiang Chinese Medical University
Jing-ming Xu
Zhejiang Chinese Medical University
Wen Mao
Zhejiang Chinese Medical University
Feng-qin Wu
Zhejiang Chinese Medical University
Hong-yuan Wang
Affiliated Hospital of Nanjing University of Chinese Medicine
Zhi-Ling Sun
Nanjing University of Chinese Medicine
Qiu-hua Sun (sunqiuhua@zcmu.edu.cn)
Zhejiang Chinese Medical University https://orcid.org/0000-0001-7916-3408

Research

Keywords: Ankylosing spondylitis, Moxibustion, Metabolomics, Proteomic

Posted Date: August 26th, 2020

DOI: https://doi.org/10.21203/rs.3.rs-62909/v1

Abstract

Background: Moxibustion is widely used in ameliorating symptoms of ankylosing spondylitis (AS). The aim of this study was to identify the potential molecular profiles of moxibustion on relieving AS mice through incorporating ultra-high-performance liquid chromatography quadrupole-time of flight mass spectrometry (UHPLC-Q-TOF/MS) based metabolomics approach and data independent acquisition-mass spectrometry (DIA-MS) based proteomic.

Methods: In this research, mice with proteoglycan-induced spondylitis (PGISp) were intervened with moxibustion for four weeks at specific acupuncture points or at non-acupuncture points. Arthritis severity, histopathological examinations, cytokines and osteoblast (OB) related genes were assessed. Protein profiling and metabolite profiling of serum of mice were examined by UHPLC-Q-TOF/MS based metabolomics technology and DIA-MS based proteomic approach. A multi-omic analysis was implemented for integrating the results of the single proteomic and metabolomic. The levels of some novel proteins in significantly enriched integrated pathways were validated by the enzyme-linked immunosorbent assay (ELISA) method.

Results: Our findings clearly indicate that acupuncture points' moxibustion can significantly decrease the arthritis index (AI) score, improve the histopathological examination and reduce the serum levels of C-reactive protein (CRP), Interferon-γ (IFN-γ), Interleukin-17 (IL-17), Alkaline phosphatase (ALP) and Osteocalcin (OCN) for AS mice. A total of 21 differentially expressed metabolites and 21 differentially expressed proteins (DEPs) were identified as potential moxibustion-intervened biomarkers for AS mice. These molecules were mainly involved in six integrative canonical pathways: mineral absorption, lipid metabolism, purine metabolism, glycolysis/gluconeogenesis, glycine, serine and threonine metabolism and phenylalanine metabolism pathways. Furthermore, The ELISA analysis of four key proteins was consistent with the results of the proteomic analysis.

Conclusions: Combing UHPLC-Q-TOF/MS based metabolomics approach and DIA-MS based proteomic, as a promising tool, can advance our understanding of potential mechanisms of action of moxibustion for AS from a holistic perspective.

Background

Ankylosing spondylitis (AS), a common spondyloarthropathy (SpA), is a systemic inflammatory disease of unknown exact causes, which affects about 0.2–1% adult population worldwide [1]. Typical clinical hallmarks of AS include inflammatory back pain, stiffness, deformity and ankylosis of the spine, synovitis in the lower limbs, fatigue and extra articular manifestations such as uveitis, inflammatory bowel disease, and psoriasis [2]. The incidence of AS is highest in male young people aged between 20 and 30 years [3]. Additionally, AS decreased patients' health-related quality of life (HRQoL), negatively affected their work performance, disturbed their body image and self-esteem, and adversely influenced their sexual activity and social interactions [4, 5].

Currently, the European League Against Rheumatism (EULAR) and the American College of Rheumatology (ACR) recommended two significant kinds of first-line treatment options available for axial manifestations of AS, initially with nonsteroidal anti-inflammatory drugs (NSAIDs) for the mild AS condition, and subsequently systematic biological agents therapies [6]. There was recognition that use of selective or non-selective NSAIDs medication might yield a beneficial effect on slowing down radiographic progression in AS patients [7]. However, these recommended NSAIDs medicines produced partial responses for AS patients with high disease activity and these agents are frequently associated with cardiovascular risk increasing and adverse gastrointestinal effects [8]. To date, several dramatic biological agents (secukinumab, etanercept, infliximab, adalimumab. etc) have shown their benefits on reducing the activity for moderate-to-severe AS patients who have had inadequate response to standard NSAIDs therapies [9]. However, the costs of these novel biological agents might be too expensive; thus, early and continuous biological therapies bring a heavy economic burden for AS patients in developing countries [10].

Therefore, consequently, more and more AS patients have turned their attention to seeking traditional Chinese medicine (TCM) intervention as an effective adjunct to pharmacological drugs in the management of AS [11]. As an important component of TCM, moxibustion is defined as heat therapy in which dried herbal preparations called "*Artemisia vulgaris*" (Ai Ye in the Chinese term) are burned directly or indirectly onto the body's acupuncture points or certain locations. According to the TCM theory, AS is attributed to damp and cold in *Du* meridians and kidney deficiency. Moxibustion may effectively warm the *Du* meridians and expel damp and cold, strengthen the body's ability to restore kidney *Yang* and promote *Qi* and blood circulation. In terms of clinical trial and systematic review, previous studies from our research team have suggested that moxibustion as an adjuvant therapy in combination with NSAIDs or biological agents may exert positive effects on improving physical function and HRQoL and reducing the disease activity and serum levels of ESR for AS patients [12–14].

As moxibustion may possess the ability to benefit AS patients, possible mechanisms of action are of interest. In Zhang *et al*'s study [15], moxibustion can inhibit non-specific endochondral ossification of spine through the regulation of C-terminal peptide and osteocalcin of type I collagen protein expression after stimulating DU14 and DU2 acupuncture points in AS patients. Additionally, in Li's study [16], moxibustion could not only down-regulate the abnormal expression of HLA-B27 gene, stabilize the balance of Th17/Treg/Th1 but also regulate the immune function by increasing the mRNA expression levels of Foxp3 and T-bet in the serum of AS patients. Some efforts have been made previously to explore the possible molecular mechanism of moxibustion intervention for AS on the basis of only a handful of DNA, mRNA or proteins. However, TCM interventions including moxibustion are complex interventions that concentrate on the organization of the entire system, rather than a single signalling pathway or a single target [17]. Thus, according to previous literature research, the global view of moxibustion effects is still lacking and it is necessary to further explore the biological mechanism of moxibustion more comprehensively and systematically.

With technological advancements in the field of system biology, 'OMICS' (genomics, transcriptomics, proteomics and metabolomics), as novel and comprehensive technologies, has been proven to result in breakthroughs in capturing the systematic picture of the complex biological processes [18]. Notably, the 'OMICS' strategy is also fully complied with the holistic and multi-target characteristics of TCM and thus may be a pivotal method for elaborating the action mechanisms of moxibustion for AS [17, 19]. Metabolomics, as an intrinsic part of the 'OMIC'method, provides a high throughput platform to expound the situation of multiple metabolic perturbations resulting from exogenous and endogenous stimulations. In comparison to DNA, mRNA or proteins, the

downstream metabolic profiles constitute one-step closer to 'phenotype', which can directly define the molecular 'phenotype' and reveal the function of cells or organisms in response to encompassing environmental alterations and multi-level regulations (DNA, mRNA, proteins etc.) [20]. Thus, metabolic profiles are sensitive indicators of the 'phenotype', which can reveal the function of biological endpoints more precisely than gene or protein analysis [21]. Previously, our preliminary urinary-based metabolomics study had revealed that moxibustion exerted its anti-AS effect mainly by modulating the TCA cycle, lipid metabolism, amino acid metabolism, intestinal flora metabolism and purine metabolism [22]. However, downstream metabolic profiles are highly variable, which can be prone to be altered by other confounding endogenous and environmental factors [23]. Proteomic, as the closest upstream regulatory layer to metabolomics, can directly modulate and affect the downstream metabolic profile expressions [24]. Therefore, integration of proteomic and metabolomic profiles may enhance the reliability in elucidating downstream metabolic alterations caused by specific upstream proteins and/or enzymatic pathways and further provide multi-omics and system-wide perspectives of the complex mechanisms of TCM interventions. Actually, in contrast to the single-omics approach, joint proteomics and metabolomics analysis has been particularly attractive in exploring the underlying biochemical mechanisms of Chinese herbals [25] or Chinese patent medicine [26]. Nevertheless, to date, the study of moxibustion by multi-omics is still scarce. Additionally, compared to the urine samples we used in the previous study [22], serum-based multi-omics study may be a better choice, because serum is less susceptible to being influenced by exogenous factors and contains more proteins [27]. Therefore, herein, we employed a serum-based multi-omics strategy through incorporating UHPLC-Q-TOF/MS based metabolomics and DIA-MS based proteomic approach to identify the possible molecular mechanisms of moxibustion for AS at system levels.

Methods

The schematic diagram of the experimental processes is shown in **Fig. 1**. The detailed experimental methods are listed one by one below.

Ethical statement

Animal care and experimental procedures were performed according to the internationally recognized ARRIVE guidelines and guidelines of the Institutional Animal Care and Use Committee (IACUC) of Zhejiang Chinese Medical University. Moreover, the ethics committee of Zhejiang Chinese Medical University approved this study protocol (No. SCXK2016-0010). All experimental procedures were based on the principles of the "three Rs" (Replacement, Reduction and Refinement).

Experimental animals and the establishment of the proteoglycan-induced AS model

Thirty-two locally supplied 3-month-old female Balb/c mice were housed in the AAALAC-accredited Experimental Animal Center at the Zhejiang Chinese Medical University in environmentally controlled conditions: temperature: (25±1) °C, relative humidity: (56±2) % and light (12 h/12 h light-dark cycle). All mice had free access to a standard chow pellet diet and water ad libitum. After a one-week adaptation, all mice were divided randomly into the healthy control group mice (HC group, *n*=8) and other mice (*n*=24), which were used for AS modelling. According to our previous published study [22] and the other published literature [28, 29], the AS mice models were induced by i.p. injection with an emulsion of 100μg of cartilage proteoglycans (PG) (Sigma-Aldrich, St. Louis, MO, USA) and 2 mg dimethyldioctadecylammonium (DDA) (Sigma-Aldrich, St. Louis, MO, USA) for 3 times at 21 days intervals. Fourteen weeks after the third i.p. injection (at 20 week), the success of AS modeling was confirmed by measurements of arthritis index (AI) score (each paw had a score over 1) and axial skeleton ankyloses through the animal digital radiography (Aolong, Dandong, China) [22, 28, 30]. Afterward, the confirming AS modeling mice were randomly divided into three groups, including untreated AS mice (AS group, *n*=8), or AS mice that received moxibustion at acupuncture points (MA group, *n*=8) or AS mice that received moxibustion at non-acupuncture points (MNA group, *n*=8) [22, 31].

Moxibustion intervention

Mice in the MA group were fixed on the platform after shaving the hair to expose the skin of moxibustion intervention region. As previously described [22, 32], the moxa cone (height: 120 mm, diameter: 7 mm, "Han Medicine", Nanyang, China) was lit and held 2 cm above the selecting acupuncture points, namely bilateral BL23 and bilateral ST36 and GV4, for approximately 35 min (including 14 min for each pair of BL23 and ST36 and 7 min for GV4). Previously, according to our previous clinical trial [13], moxibustion at BL23 and ST36 and GV4 acupuncture points have been proven to ameliorate the disease activity and improve the physical function for AS patients. The selecting acupuncture points were located in accordance with the "Veterinary Acupuncture & Moxibustion Atlas" [33]. BL23 is located below the spinous process of the second lumbar vertebra (L2), 1.5cun lateral to the posterior midline. ST36 is located posterolateral to the knee about 5 mm below the fibular head. GV4 is located on the posterior midline, in depression below the spinous process of the second lumber vertebra. The moxibustion intervention was performed for 7 consecutive days in a course with a total of four courses. The non-acupuncture points at the base of the tail were used as controls [34, 35]. In addition, in order to avoid the tail acupuncture points located at distal region of the tail, moxibustion was perform at one-fifth point of tail length from the proximal region of the tail [34, 35]. These non-acupuncture points do not overlap with any other known acupuncture points. In addition to acupuncture point selection, the moxibustion intervention method was performed by the same protocol as the MA group. The mice in the control and model groups were also fixed on a board similar to that in the MA and MNA groups, but did not receive moxibustion stimulation.

Arthritis severity, biological sample collections, histopathology, cytokines and OB related genes

In order to record the effects of moxibustion on arthritis severity in mice paws, the AI score in each mouse was recorded by the same observers, who were blind to the group allocation as previously described [29, 32]. The maximum AI score per paw was 4 and the maximum AI score per mice was 16 [29, 32]. The detailed criteria about the AI scoring system was described in **Additional file 1: Table S1.** Under anesthesia using isoflurane, blood samples were collected through cardiac puncture. The serum was separated by centrifuging at 3000× g for 15 min and the supernatants were stored at -80 °C. After sacrificing all mice, dissected left ankle joints were fixed with 10% formalin (v/v) for 1 day, decalcified with 5% formic acid (w/v) for 30 days and dehydrated by application of ethanol. After that, dehydrated specimens were processed for paraffin embedding, cut into 5 μm thin slices and stained with hematoxylin-eosin (H&E). Subsequently, these stained slices were imaged with the Virtual Slide Scanner NanoZoomer 2.0-HT (Hamamatsu Photonics, Hamamatsu, Japan). An

experienced pathologist, who was blinded to the group allocation, assessed the slides in accordance with cartilage destruction, inflammatory cell infiltration, the narrowing of joint space and synovial hyperplasia as previously described [22, 28, 29]. For measuring cytokines and OB-specific genes' levels, the serum concentrations of CRP, IFN-γ, IL-17, ALP and OCN were detected using commercial ELISA kits (MEIMIAN, Yancheng, China) following the manufacturer's instruction.

UHPLC-Q-TOF/MS based metabolomics analysis

Sample Preparation for Metabolomics Study

The freeze serum samples were thawed at 4 ℃ temperature. Next, 100μL serum from each sample was mixed with 400μL precooled solution (methanol: acetonitrile, 1:1, v/v). Then, in order to precipitate proteins, the mixture solution was incubated for one hour at -20 °C after vortex-mixing for 60 s. Subsequently, the solution was centrifugated at 4°C (14,000 × g for 20 min). Lastly, the supernatant was piped into tubes for lyophilization and then mixed with solution containing acetonitrile and H_2O (1:1, v/v), which was then ready for UHPLC/Q-TOF-MS analysis.

Chromatography

Metabolomics analysis was performed using an Agilent 1290 Infinity UHPLC system. (Waters Corporation, Milford, USA). The serum chromatographic separation was carried out at 25°C on ACQUITY UPLC BEH Amide (1.7 μm, 2.1 × 100 mm column) and ACQUITY UPLC HSS T3 (1.8 μm, 2.1 × 100 mm column). The flow rate was set at 0.3 mL/min. The optimal mobile phase was composed of eluent A (ddH_2O+25 mM ammonium acetate+25 mM ammonia) and eluent B (acetonitrile). The gradient elution programs for the serum were set according to our previous study [22]. The QC samples after every 8 detected samples were used to test the suitability and consistency of the LC-MS system.

Mass spectrometry

The AB Triple TOF 6600 (AB Sciex Corporation, Framingham, MA, USA), operating in both positive and negative ion modes, was applied to electrospray ionization (ESI)-Mass spectrometry (MS) experiments. The key corresponding MS conditions were set as follows: Ion Source Gas1 (Gas1): 40, Ion Source Gas2 (Gas2): 80, Curtain gas (CUR): 30, source temperature: 650°C, Ion Sapary Voltage Floating (ISVF)±5000 V (in ESI+ and ESI- mode); The information-dependent basis (IDA) method based on Analyst TF 1.7 software (AB Sciex Corporation, Framingham, MA, USA) was used for MS acquisition. The mode was set as Declustering potential (DP):±60 V(in ESI+ and ESI- mode), Collision Energy: 35±15 eV. The IDA was set as exclude isotopes within 4 Da, Candidate ions to monitor per cycle:10.

Statistical analysis

The acquired raw UHPLC-Q/TOF-MS data from serum samples were first converted to the common .mzXML format by utilizing ProteoWizard software. Then, these converted datasets were processed using XCMS Online program (http://metlin.scripps.edu) for peak identification and matching, alignment, peak filtration, and translating into the three-dimensional (retention time, mass, intensity of the peaks) data matrices [36]. Subsequently, the resulting dataset of each sample was normalized and transformed by log with Metaboanalyst 4.0 (Montreal, Quebec, Canada) [37]. After that, these resulting data matrices were imported into SIMCA-P 14.0 software package (Umetrics AB, Umeå, Sweden) for a series of multivariate statistical analysis (MVA) after pareto-scaling. Firstly, a partial least squares discriminant analysis (PLS-DA) was performed to overview the metabolic profile differences among four groups. Next, the supervised orthogonal projection to latent structure-discriminant analysis (OPLS-DA) was utilized to distinguish different groups. A permutation test (200 permutations) was used to confirm the validity of the MVA model against over-fitting. Moreover, the quality of the MVA model was evaluated by the R^2 (cum) and Q^2 (cum) values. The potential metabolic candidates were filtered based on the following: Benjamini-Hochberg's False Discovery Rate (FDR) correction<0.05 in one-way analysis of variance (one-way ANOVA) followed by Tukey's HSD comparison test using GraphPad Prism 8 software packages (San Diego, California, USA), fold change (FC) >1.33 or <0.77, variable importance for project (VIP) values of the established OPLS-DA model > 1 and the correlation coefficient |r| of the established OPLS-DA model >0.55 [38]. Then, as described in the previous research [39], the enhanced four-dimensional volcano plot including the parameters from the univariate analysis ($\log_2$ FC, –log(*p*-value)) and multivariate analysis (VIP and correlation coefficient (|r|) values of the established OPLS-DA model) were conducted to reflect the potential discriminating variables among the different groups.

Metabolites identification and metabolic pathway analysis

The structure of metabolites was identified by accurate mass number matching (< 25 ppm) and secondary spectrogram matching. The LC/MS spectra was assigned according to the freely accessible online biochemical databases (HMDB, METLIN, KEGG etc.) and in-house developed LC/MS databases.

MetPA (Metabolomics Pathway Analysis) was used for holistic PATHWAY analysis. In the pathway analysis algorithms model, "hypergeometric test" and "relative-betweeness centrality" were selected for performing over-representation analysis and pathway topology analysis, respectively. Moreover, the KEGG category was chosen as the pathway library model. The threshold of the raw *P*-value was set as 0.05 to filter out the most important and potential relevant metabolic pathways.

DIA-MS based proteomics analysis

Sample Preparation and Fractionation for DDA library Generation

Firstly, in order to effectively expand and improve the dynamic range, 150 μl of pooled serum from each group was immunodepleted for removal of top 14 high abundant proteins using a commercial depletion kit (MARS™, Agilent Technologies) coupled to a High-Performance Liquid Chromatography (HPLC, Shimadzu LC-10AT). High abundant proteins depletion was performed according to the manufacturer's protocols and buffer exchange was employed with 25

mM ammonium bicarbonate (ABC) in ddH_2O using ultrafiltration devices with a 10 kD molecular weight cut off (Microcon, Millipore-Merck, Germany). After collecting the resulting protein solution, the total protein concentrations were quantified with a Bicinchoninic acid protein assay (Thermo, IL, USA) according to the manufacturer's instructions.

Secondly, the serum protein digestion steps were carried out following the Filter-Aided Sample Preparation approach [40]. In short, protein concentrates (200 μg) were lysed directly using 30 μl of STD lysis buffer (4% [w/v] SDS, 100 mM Dithiothreitol in 0.15 M Tris pH 8.0). Afterward, excess reagents in the resulting lysates of serum samples were depleted using UA solution (8 M Urea in 0.15 M Tris pH 8.0) by repeated ultrafiltration (30 kDa cut-off, Microcon, Millipore-Merck, Germany). After that, 100 μl of UA buffer containing 0.05 M iodoacetamide (IAA) was mixed with the filters, and the sample mixtures were incubated at room temperature for 30 min in darkness. Subsequently, filter units were washed three times with 100 μl of UA buffer and then twice with 100 μl of 25 mM Ammonium Bicarbonate (Sigma, MO, USA). Finally, each filter unit was sequentially digested with 2 μg trypsin (Promega, Madison, WI, USA) in 40 μl of 100 mM Ammonium Bicarbonate buffer and the mixture solution was incubated overnight at 37 °C. All resulting tryptic peptides were then collected via centrifugation. Peptide content was estimated by UV light spectral density at 280 nm.

Thirdly, pooled tryptic peptides were next fractionated using a commercial peptide fractionation kit (Pierce™ High pH Reversed-Phase Peptide Fractionation Kit, Thermo Fisher Scientific). Each fraction was concentrated by vacuum centrifugation (Benchmark Scientific, NJ, USA) and further acidified with 10μl of 0.1% (vol/vol) formic acid. Afterwards**,** all resulting peptides were acidified with 40μl of 0.1% (v/v) formic acid prior to desalting with C18 Cartridges (Empore™ SPE Cartridges C18 (standard density), bed I.D. 7 mm, volume 3 ml) according to the manufacturer's protocol (Thermo Fisher Scientific, MA, USA) [41].

Fourthly, the iRT-Kits (Biognosys, Schlieren, Switzerland) were added into the pooled digest serum samples to normalize the relative retention time.

DDA Mass Spectrometry Assay

All fractions were used for generating an extensive serum-specific DDA library. As previously described, DDA Mass Spectrometry Assay was carried out with the help of a Thermo Scientific Q-Exactive HF mass spectrometer connected to an Easy-nLC™ 1200 chromatography equipment (Thermo Scientific, MA, USA) [41]. Firstly, two micrograms of peptides were re-dissolved in 2% (v/v) ACN and 0.1% (v/v) FA, and then pooled tryptic peptide samples were injected into an EASY-SprayTMC18 Trap column (Thermo Scientific, P/N 164946, 3um, 75um*2cm). Subsequently, a 120-minute segmented gradient of solvent [80% (v/v) ACN and 0.1% (v/v) FA] at a flow rate of 250 nl/min on an EASY-Spray^{TM}C18 LC Analytical Column (Thermo Scientific, ES803, 2um,75um*50cm) was used for peptide separation. Afterwards, eluting peptides were detected by mass spectrometry analysis in an ESI^+ ion model. The parameters for one MS survey scan experiment were set as follows: (1) The mass range: m/z 300–1,650 Da; (2) High resolution, R: 60,000 (FWHM) at m/z 200; (3) Dynamic exclusion: 30s; (4) AGC (Automatic gain control) target for MS: 3×10^6; (5) Maximum IT: 25 ms. Each full MS SIM scan followed 20 dd-MS2 scans, and the parameters for tandem MS/MS scans experiments were set as follows: (1) High resolution, R: 15, 000 (FWHM) at m/z 200; (2) AGC target for MS2: 5×10^4; (3) Maximum IT: 25 ms; (4) Fragmented by normalized collision energy (NCE): 27 eV.

Mass Spectrometry Assay for DIA

Each sample peptide was analyzed by LC-MS/MS performing in the DIA mode with the Q-Exactive HF mass spectrometer (Thermo Scientific, MA, USA) by Shanghai APT proteomic institute (Shanghai, China). In the DIA analysis, each DIA cycle comprised of one full MS–SIM scan with m/z 15 Da per isolation window to cover the scan range of m/z 350–1,650 Da [42]. The experimental set-up conditions for the DIA analysis were almost similar to the DDA analysis. The MS1 scans were set as: (1) High resolution, R: 60,000 (FWHM) at m/z 200; (2) AGC target for MS: 3×10^6; (5) Maximum IT: 50 ms and profile mode. MS2 scans were set as: (1) High resolution, R: 30, 000 (FWHM) at m/z 200; (2) AGC target for MS2: 3×10^6; (3) Maximum IT: auto; (4) Fragmented by NCE: 30 eV. Moreover, equal aliquot of each sample from all groups were pooled as QC samples were injected with DIA mode at the beginning of the LC-MS/MS analysis. The QC samples after every 4 detected samples were used to examine the suitability and consistency of the LC-MS system.

Mass spectrometry data analysis

For protein quantification, DDA library data files were processed with MaxQuant analysis software (version 1.5.3.17), which performed a tandem mass spectrometry (MS/MS) spectra search against the combined databases of FASTA sequences and iRT standard peptide sequences. Searching parameters were set as follows: (1) Enzyme specificity: full tryptic//P digestion; (2) Control modification: carbamidomethylation of cysteine (C); (3) Dynamic modification: N-acetylation (N-term) of proteins and oxidation of Methionine (M); (4) Tryptic peptides: no more than 2 missed cleavages; (5) The satisfy FDR: ≤ 1% at peptide level. For generating a reference DDA spectral library, the original raw files and DDA searching results of each sample were imported into the Spectronaut Pulsar X^{TM} (version 12.0.20491.4) software (Biognosys, AG, Switzerland). The building DDA spectral library was next normalized to iRT standard peptides.

Subsequently, Spectronaut Pulsar X^{TM} (version 12.0.20491.4) software (Biognosys, AG, Switzerland) was applied to match the original DIA-MS data against the above constructed DDA spectral library. The parameters were set as follows: (1) RT prediction type: Dynamic iRT; (2) Interference correction on MS2 level; (3) Cross run normalization. All results were quantified and filtered based on adjusted Q value < 0.01 criterion.

Protein identification and bioinformatics methods

The DEPs were filtered by Benjamini-Hochberg's FDR correction<0.05 in one-way ANOVA followed by Tukey's HSD comparison test using GraphPad Prism 8 software packages (San Diego, California, USA) as well as FC >1.33 or <0.77 [32].

In order to determine the functional classification and functional enrichment of DEPs altered in the serum of AS mice by moxibustion interventions, Database for Annotation, Visualization and Integrated Discovery (DAVID) v6.8, an online functional annotation tool, was adopted to perform a Gene Ontology (GO) enrichment analysis. Biological Networks Gene Ontology (BiNGO), a plug-in in a cytoscape visualization platform software (version 3.7.2, free available from

http://www.cytoscape.org/), was employed to further annotate functional Go terms into three categories, including biological functions, molecular function and subcellular locations [43]. Canonical pathway enrichment analysis of DEPs was carried out using the Kyoto Encyclopedia of Genes and Genomes (KEGG) (https://www.kegg.jp/) automatic annotation server and REACTOME (https://reactome.org/) databases. FDR values less than 0.05 were considered to indicate statistically significant enriched GO terms or associated canonical pathways. The Protein-Protein interaction (PPI) network was established by STRING online software.

Validation of DEPs

Four of the DEPs identified by the DIA-MS based proteomic analysis (LCAT, TF, HSPA8 and MIF) were validated using commercial enzyme-linked immunosorbent assay (ELISA) kits (MEIMIAN, Yancheng, China) according to the manufacturer's instructions. The OD value was read at 450 nm with a PerkinElmer EnSpireTM multilabel reader (PerkinElmer Life and Analytical Science, Turku, Finland).

Integrated analysis of metabolomics and proteomics

A multi-omic analysis was implemented for integrating the results of the single proteomic and metabolomic. According to the data of proteomics and metabolomics platform, MetaboAnalyst 4.0 was carried out to acquire the integrated canonical pathway. The significantly enriched integrated pathways were filtered after examining a threshold of FDR <0.05. The correlation network diagram established by OmicBean software (a web-based software application for interacting multi-omic data and available from http://www.omicsbean.cn/) can display moxibustion-intervened differentially expressed metabolites, DEPs, and significantly perturbed signaling pathways through visual interaction. The protein–metabolite interaction network was generated with a score of ≥ 2, number of nodes>60 and p-value < 0.05 [44]. Finally, the hierarchical cluster analysis of identified proteins and metabolites was employed by MEV software (version 4.9.0).

Afterward, the Pearson correlation matrix analysis approach through Correlation Calculator (version 1.0.1) was performed to explore the correlations between the potential biomarkers including validated proteins, significant metabolites and biochemical indicators [45]. A value of $p<0.05$ was considered statistically significant.

Results

AI score, the histological examinations, and expression of inflammatory cytokines and OB related genes

In line with the literature [28, 30], fourteen weeks after the third i.p. injection (at week 20), mice in the AS, MA and MNA group showed significant increasing levels of AI score when compared with the HC group ($p<0.01$). Before performing the moxibustion (at week 20), there were no statistically significant differences among the AS, MA and MNA group in terms of the levels of AI score ($p>0.05$). However, compared with the AS group, the AI score in the MA group was significantly decreased after 4-week moxibustion therapy ($p<0.05$). (**Fig. 2A**).

As shown in **Additional file 1: Figure S1**, histopathological results of the left ankle joint from AS model group (**Figure S1 B**) showed cartilage enlargement and erosion, inflammatory cell infiltration and narrowing the joint space compared with those in the control group. Moreover, compared with the AS group, both MA group and MNA group can remarkably inhibit the narrowing of joint space in AS mice (**Figure S1C and Figure S1D**). However, compared with the MNA group, there is more significant improvement in synovial hyperplasia, inflammatory cell infiltration and cartilage defection of AS mice with moxibustion at specific acupuncture points (**Figure S1 C**). It suggests that moxibustion intervention at specific acupuncture points had a relatively better effect on ameliorating the arthritic characteristics in AS mice.

As shown in the **Fig. 2 B-F**, the serum levels of CRP, IFN-γ, IL-17, ALP and OCN in the AS group were significantly increased as compared with the HC group ($p<0.01$). However, compared with the AS and MNA group, moxibustion on the GV4, BL23 and ST36 acupuncture points significantly decreased the serum levels of CRP, IFN-γ, IL-17, ALP and OCN ($p<0.01$). Compared with the AS group, moxibustion on non-acupuncture points had favorable but not statistically significant effects in reducing the serum levels of CRP, IFN-γ, IL-17, ALP and OCN ($p>0.05$).

UHPLC-Q-TOF/MS based metabolomics results

UHPLC/Q-TOF-MS method validation

In order to eliminate system technical errors, the relatively clustering of QC samples was calculated to examine the repeatability and robustness of the UHPLC/Q-TOF-MS metabolomics method. As shown in **Additional file 1: Figure S2**, all of the four QC samples in both ESI+ and ESI- ion modes were less than 2 SD, indicating that the data from the UHPLC/Q-TOF-MS metabolomics were reliable [46].

Pattern recognition analysis

The representative UHPLC/Q-TOF-MS total ion chromatogram (TIC) profiles of serum samples in ESI+ and ESI- mode are shown in **Additional file 1: Figure S3.** Although the TICs were quite different from the ESI+ to ESI- mode, visual inspection of TICs in the same ESI+ or ESI- mode of HC, AS, MA and MNA groups showed less clear differences. Thus, MVA, including PLS-DA and two-group of OPLS-DA, was used to further discover any potential endogenous metabolites related to AS and moxibustion treatment.

PLS-DA was first utilized to overview the metabolic profile differences of serum samples among different groups. PLS-DA of serum dataset showed a clear group separation among HC, AS, MA and MNA groups in both ESI+ and ESI- modes (**Fig. 3**). Moreover, according to **Fig. 3**, variations of serum metabolic profiling in the MA group were much closer to the HC group than others; whereas scattered points from the MNA group were much closer to the AS group than

the MA group. Therefore, metabolic perturbations caused by the AS modeling had the tendency to be reversed moving towards to the normalized state following moxibustion at specific GV4, BL23 and ST36 acupuncture points, but little influenced by non-acupuncture points moxibustion intervention.

Identification of potential serum biomarkers and the changing trends among different groups

Herein, pairwise comparisons using the OPLS-DA model were further performed to elucidate the potential biomarkers that were responsible for the pathological process of AS and possible anti-AS mechanism of moxibustion intervention in serum samples. After pareto scaling, OPLS-DA score plot showed good separations between HC vs. AS (**Fig. 4A and 4B**) and AS vs. MA (**Fig. 4C and 4D**) in both ESI+ and ESI- mode. The cumulative R^2Y and Q^2 of OPLS-DA model in ESI+ and ESI- modes suggested that the models were good to prediction and reliability [47] (HC vs. AS: ESI+: R^2Y=0.998 cum, Q^2=0.870 cum; ESI-: R^2Y=0.999 cum, Q^2=0.890 cum. **Fig. 4A and 4B**; AS vs. MA: ESI+: R^2Y=0.989 cum, Q^2= 0.706 cum; ESI-: R^2Y=0.989 cum, Q^2=0.645 cum. **Fig. 4C and 4D**). Moreover, a permutation test (200 iterations) also showed that the results of OPLS-DA models were robust and low risk of over-fitting (HC vs. AS: ESI+: R^2=0.998, Q^2=0.870; ESI-: R^2= 0.999, Q^2=0.890. **Additional file 1: Figure S4A and S4C**; AS vs. MA: ESI+: R^2=0.989, Q^2=-0.706; ESI-: R^2=0.989, Q^2=0.645. **Additional file 1: Figure S4B and S4D**). Then, the enhanced four-dimensional volcano plot revealed a number of metabolic features that were responsible for the differences among different groups. In this study, 61 discriminatory endogenous metabolites were ultimately screened out which showed significant alterations between HC and AS groups according to the pre-defined criteria. Notably, MA intervention remarkably regulated 21 of 61 metabolites (Benjamini-Hochberg's FDR correction<0.05, AS vs. MA in one-way ANOVA followed by Tukey's HSD comparison test) (**Fig. 4E** and **Table 1**). Histograms of all 21 differential metabolites in both ESI+ and ESI- mode were shown in **Additional file 1: Figure S5**, which included 2 elevated metabolites and 19 decreased metabolites. Additionally, 9 metabolites (phosphorylcholine, glucose 6-phosphate, L-Phenylalanine, allantoin, serine, ethanoic acid, D-Mannose, L-Malic acid and citrate) were significantly altered in both MA and MNA groups compared with the AS group, most of which were associated with the TCA cycle and energy metabolism (**Additional file 1: Figure S5** and **Table 1**). Finally, the clustering heat-map showed the trends of the serum metabolic concentration difference among different groups (**Fig. 4F**).

Metabolic pathway analysis

As shown in **Fig. 5**, 21 endogenous metabolites listed in **Table 1** primarily involved in Glyoxylate and dicarboxylate metabolism, Aminoacyl-tRNA biosynthesis, Phenylalanine, tyrosine and tryptophan biosynthesis, Phenylalanine metabolism, Glycine, serine and threonine metabolism, Glycerophospholipid metabolism, Citrate cycle (TCA cycle), Purine metabolism and Pyruvate metabolism.

DIA-MS based Proteomics results

Expressions of moxibustion-associated proteins in the serum of AS mice

DIA-MS based proteomic platform was used to comprehensively profile the moxibustion-trigged protein expression in the serum of AS mice. To minimize biological variation, two or three serum samples were pooled together to acquire three biological replicates for each group. Ultimately, DIA-MS based proteomic analysis, identified a total of 7,614 peptides, corresponding to 486 proteins across pooled serum samples from the HC, AS, MA and MNA groups. Then, 439 of 486 proteins were successfully quantified for further statistical analysis. Following the pre-defined criteria, 34 DEPs were regarded as potential proteomic profiles of PG-induced AS with FDR <0.05 (HC vs. AS in one-way ANOVA followed by Tukey's HSD comparison test), and FC>1.33 or <0.77. Importantly, 21 of 34 proteins in the serum of AS mice were significantly reversed after moxibustion intervention at GV4, BL23 and ST36 acupuncture points (FDR <0.05, AS vs. MA in one-way ANOVA followed by Tukey's HSD comparison test), which included 6 up-regulated proteins and 15 down-regulated proteins (**Table 2**). The hierarchical clustering of these 21 candidate proteins revealed that the HC, AS, MA and MNA groups were considerably variable from each other (**Fig. 6**). While, only 4 of 21 proteins in the serum of AS mice (PSMA3, APOB, XDH and PGAM1) were significantly altered in both MA and MNA groups compared with the AS group, most of which were involved in the proteasome pathway and energy metabolism (**Table 2**).

Next, GO annotation was further performed to elaborate the sophisticated biological functions, molecular functions and subcellular localization of 21 target proteins of moxibustion intervention applied to the serum of AS mice. Totally, 631 biological functions terms, 111 molecular function terms, and 69 subcellular localization terms were significantly enriched after screening with a threshold of FDR<0.05. The top 10 most enriched Go terms for each category are shown in **Fig. 7**. Notably, most of the enriched biological function terms were concentrated in the lipoprotein metabolic process and inflammatory response **(Fig. 7A)**. The molecular function terms affected by moxibustion intervention primarily involved in threonine peptidase activity, lipid and cholesterol metabolic process, xanthine oxidase activity and protein binding **(Fig. 7C)**. In terms of the subcellular localization category, extracellular space, lipoprotein particle and proteasome complex comprised the most enriched terms **(Fig. 7E)**. Then, these top 10 statistically significant GO terms in each category (biological functions, molecular functions and subcellular localization) and their relationship with adjacent functional terms in Biological Networks were visually by BiNGO, a plug-in Cytoscape software. (**Fig. 7B, 7D and 7F**).

Furtherly, in order to gain insights on the pathway alterations associated with the moxibustion intervention, the KEGG enrichment analysis was performed with the aid of Omicbean software. The results showed that multiple canonical pathways were altered, and most of them were associated with the metabolic pathways (10%)**,** cholesterol metabolism (8%) and proteasome (6%) (**Fig. 8A**). Moreover, the bubble plot further revealed that the statistically significant canonical pathways that include 21 DEPs contributing to the effect of moxibustion were cholesterol metabolism, proteasome, ferroptosis, legionellosis, caffeine metabolism, sulfur metabolism, ubiquinone and other terpenoid-quinone biosynthesis, phenylalanine metabolism, protein processing in endoplasmic reticulum and vitamin digestion and absorption (**Fig. 8B**). Finally, the Protein-Protein interaction (PPI) network of 21 altered proteins affected by moxibustion intervention is depicted in **Additional file 1: Figure S6**.

Integrated pathway and network analysis and validation of DEPs via ELISA

For better explorations on the moxibustion-targeted molecular information, we integrated metabolomics and proteomics data, to obtain shared canonical pathways and interaction networks between these significantly altered small molecular metabolites and proteins with MetaboAnalyst 4.0 and OmicBean software. Overall, 27 significantly integrated pathways were identified with $p<0.05$, whereas 7 canonical pathways comprised both proteins and metabolites (**Fig. 9A** and **Table S2**). Interestingly, most of altered canonical pathways were related to the metabolic pathways, which are somewhat in line with the results from the single proteomics or metabolomics analysis. Our previous study used a 2 DE combined with MALDI-TOF-MS/MS technique to explore potential biomarkers of moxibustion a CIA rat model [32]. The results suggested that the metabolic pathway was the most important biological pathway involved in the regulation of moxibustion, which was also somewhat consistent with the present study.

In addition, the predicted network diagram was shown in **Fig. 9B**, the altered 18 metabolites including inosine, hypoxanthine, xanthine, glycine, xanthosine, uracil, citric acid, L-Phenylalanine, tyrosine, L-Histidine, Sn-Glycerol 3-phosphoethanolamine, glycerophosphocholine, serine, taurine, glucose 6-phosphate, citric acid, D-mannose, ethanoic acid, and L-Malic acid and the 16 of DEPs including XDH, TF, HP, HPX, CP, ORM1, HSPA8, VCP, PSMB2, PSMA6, PSMA3, LCAT, APOC1, APOA2, APOB, PGAM1, which were identified as being mainly involved in purine metabolism, mineral absorption, phenylalanine metabolism, cholesterol metabolism, glycine, serine and threonine metabolism, glycolysis or gluconeogenesis and glycerophospholipid metabolism were closely associated with the anti-AS effect of moxibustion.

Notably, according to the **Fig. 9B**, LCAT, the only detected protein in the glycerophospholipid metabolism pathway, was also involved in another enriched pathway: cholesterol metabolism pathway. Similarity, glycine, serine and threonine metabolism pathway and glycolysis or gluconeogenesis pathway shared the common protein: PGAM1. Moreover, XDH, which has a direct link to the several metabolites (uric acid, xanthine and hypoxanthine) that included in the purine metabolism pathway, may also play a vital role in the predicted protein-metabolite network. Moreover, TF and HSPA8 have the greatest number of close connections and interactions with the downstream proteins of the mineral absorption pathway. Specially, HSPA8 has the closest relationship with the PSMB2, PSMA6, and PSMA3, which are the crucial proteins involving in the proteasome pathway. MIF, the only detected protein in the phenylalanine metabolism pathway, can independently predict radiographic progression in the spine of AS. Thus, the above important proteins may play a domain role in this predicted protein-metabolite network. However, only LCAT, TF, HSPA8 and MIF are meridian specific proteins (**Table 2**). Thus, the above four key proteins in the predicted network were chosen to be further validated by ELISA. The ELISA results revealed that four DEPs were significantly up-regulated (LCAT and HSPA8) or down-regulated (TF and MIF) in the serum of the MA group compared with the AS model group (**Fig. 10**), consistent with DIA-MS based proteomic analysis.

Correlation between potential biomarkers and biochemical indicators

The results of correlation analysis between potential biomarkers and biochemical indicators in serum were shown in **Additional file 1: Figure S7**. At the protein level, TF was positively and highly correlated with IFN-γ, IL-17 and AI score and MIF had a remarkable positive correlation with CRP. However, LCAT was negatively correlated with IFN-γ in our research. Moreover, TF and MIF showed obvious positive correlation with all OB-specific genes including ALP and OCN. At the metabolic level, there was a significant positive correlation between taurine and cytokines such as CRP and IL-17. However, tyrosine and D-Mannose were negatively related to the inflammatory measurements. Moreover, L-phenylalanine was closely related to the OB-specific gene ALP.

Discussion

Similar to our previous studies [22, 32], the findings of this study clearly indicate that acupuncture points' moxibustion can significantly improve the inflammatory status of AS mice, which includes decreasing the AI score and reducing the serum levels of CRP, IFN-γ, IL-17 in AS mice. Moreover, moxibustion at specific GV4, BL23 and ST36 acupuncture points also improves histopathological examinations and decreases the serum levels of OB-specific genes, including ALP and OCN for AS mice. According to results of metabolomic and proteomic studies, 21 differentially expressed metabolites and 21 DEPs were identified as potential moxibustion-intervened biomarkers for AS mice. Furthermore, the predicted protein-metabolite network showed that six altered canonical pathways, including mineral absorption, lipid metabolism, purine metabolism, glycolysis/gluconeogenesis, glycine, serine and threonine metabolism and phenylalanine metabolism pathways, were closely related to the anti-AS effect of moxibustion. The details will be further discussed accordingly.

Mineral absorption

As depicted in **Fig. 9B**, ten proteins (TF, Hp, Cp, ORM1, HPX, HSPA8, VCP, PSMB2, PSMA6, and PSMA3) alone with one metabolite (Citrate) were altered by moxibustion.

Previously, several acute-phase reactants, including serotransferrin (TF), are over-expressed in the PBMCs of AS patients compared with healthy controls, and anti-TNF-α agents significantly decreased the levels of TF in AS patients [48, 49]. In the present study, the serum level of TF increases in AS modeling mice compared with HC mice, and it decreases markedly after 4-weeks' moxibustion intervention, which is in line with the previous clinical studies. Thus, moxibustion may also have a direct effect on decreasing the acute-phase protein levels in AS. Meanwhile, TF is an iron-regulator protein which can mediate the uptake of iron in many cells. The previous research had revealed that there was a negative correlation between the levels of iron ion and the serum TF in Sprague–Dawley rats [50]. In this study, the significantly decreasing expression of TF that is regulated by moxibustion intervention may contribute to the increasing the concentrations of iron, which is consistent with results from the anti-TNF therapy in the previous clinical report [49]. Using vitro murine calvarial MC3T3-E1 OB cells culture system, Yamasaki *et al.* [51] had revealed that high concentrations of iron could prohibit the proliferation, differentiation and deposition of calcium in MC3T3-E1 OB cells. Notably, AS is specifically characterized by OB activity and bone resorption increasing [52, 53]. Thus, moxibustion may suppress the OB activity, calcification and mineralization for AS mice by reducing the serum levels of TF, which is further verified by the down-regulation of the OB specific gene (ALP and OCN). (**Fig. 10** and **Additional file 1: Figure S7**)

In addition to TF, other acute-phase proteins in the mineral absorption pathway such as Hp, Cp and ORM1, were also up-regulated in AS modeling mice. Hp plays a significant role in modulating immune and inflammatory responses on various immune cells (neutrophils, macrophages, lymphocytes, etc.).

Previously, Li *et al*. had reported an up-regulation of Hp levels in patients with AS, but the serum levels of Hp are not strongly correlated with the disease activity of AS [54, 55]. Cp is a kind of metal proteins, involving in excretion of copper, copper-dependent oxidation, and iron transporting [56]. A great number of studies had already reported that the serum level of Cp was over-expressed in patients with rheumatic conditions (including AS) compared with healthy individuals, which was consistent with the results of our current study [57, 58]. ORM1 is a transport protein which is involved in regulating the activity of the immune system during the acute-phase reaction. Additionally, combined serum levels of ORM1, Apcs, and CRP were shown to have a high value for diagnosing AS [59]. However, moxibustion intervention can apparently reverse the over-expression levels of these three acute-phase proteins, suggesting that moxibustion plays a critical role in decreasing the acute phase process of AS.

Hemopexin (HPX), primarily a heme binding protein, is frequently secreted during inflammatory responses. Using iTRAQ-based proteomic approach, Cai *et al*. [28] had demonstrated that compared with the healthy volunteers, the HPX protein was found to be over-expressed in PBMCs of AS patients, which was in line with the results of our current study. To explore this issue, HPX was known as a 'toxic heme' transporter and scavenger in the blood, thus the up-regulating of HPX in AS could protect cells against oxidative stress [60, 61]**.** In this research, the serum level of HPX is further elevated after moxibustion at GV4, BL23 and ST36 acupuncture points, suggesting that moxibustion is able to promote the host defense and inhibit oxidative stress for AS. Also, another previously published proteomic study from our research team had supported a significant increase in the HPX concentration after moxibustion in the collagen-induced arthritis (CIA) rat [62].

HSPA8 is a type of heat shock proteins (HSPs). The upregulation expression of HSPs may exert a protective effect on organisations by stabilizing the protein structure, inhibiting the release of proinflammatory cytokines (TNF-α, IL-1β, IL-6, etc.) and modulating the host immune response, especially during the chronic stress condition [63]. Of note, HSPs may also serve as crucial roles involved in the mechanism of action of moxibustion [64]**.** Previously, Yi *et al* [65] and Chang *et al* [66] proved that moxibustion at ST36 and ST21 acupuncture points could protect gastric mucosal cells against stress injury by increasing the levels of HSPs. Moreover, our previous proteomic study [32] also had proven that moxibustion at ST36 and BL23 acupuncture points could elevate the serum levels of HSPs, which played a key role of anti-arthritis in the CIA rat. Consistent with these previous reports, in this study, the serum concentration of HSPA8 has increased markedly following moxibustion intervention at GV4, BL23 and ST36 acupuncture points, and AI score reduction (**Fig. 2A**) and ankle pathological improvement (**Additional file 1: Figure S1**) also have been observed in the MA group than in the AS model group, implying the protecting effect of moxibustion on musculoskeletal damage in AS mice.

Based on our studies, three main downstream enzymes (PSMB2, PSMA6 and PSMA3) of HSPA8, were found to be over-expressed in the serum of AS mice. Notably, these proteins are involved in the proteasome pathway that we have found in the proteomic KEGG enrichment analysis (**Fig. 8B**). These results, somewhat, consist with that of Write *et al* [67] who reported that proteins involved in the proteasome pathway were up-regulated in the monocytes of AS patients. To explore this issue, proteasome is a proteolytic enzyme complex existing in the cytoplasm and nucleus, which is responsible for degrading most proteins in the cell, and plays a key role in the expression of MHC class I molecules (including B27 molecules) and antigen presentation [68]. However, the activation of proteasome could degrade MHC class I molecules produce antigen arthritic peptides that can bind to their own B27 molecules, and further present to CD8 cytotoxic T cells, thereby initiating the pathogenesis of AS. In the present study, moxibustion at proper acupuncture points could prohibit the activation of proteasome pathway via downregulating the expression of PSMB2, PSMA6 and PSMA3 and played a role of anti-AS [69].

Citric acid is a vital intermediate of the TCA cycle and the VCP is primarily involved in the ATP metabolic process. Both of them play a prominent role in the metabolism of energy. It had been well reported that metabolites and proteins involved in the TCA cycle were significantly raised to enhance energy production, so as to compensate for insufficient energy sources caused by glycolysis under AS inflammation condition [70]. Similarity, in this study, the levels of citric acid and VCP increased in the PG-induced AS model mice group compared with the healthy control group, suggesting a boosted energy supply to compensate for the shortage of body energy. Previously, our research team had demonstrated that moxibustion could correct abnormal energy metabolism in CIA through down-regulating the plasma levels of VCP [32]. Moreover, the urine level of citric acid has also been proven to down-regulate significantly following moxibustion intervention in AS mice [22]. Consistent with these findings from our previous research, herein, by means of acupuncture point's moxibustion intervention, decreased serum levels of citric acid and VCP are observed in this study, which indicate that moxibustion at specific acupuncture points can contribute to reducing the symptoms of AS by recovering the impairment of energy metabolism.

Lipid metabolism pathway

In this research, the molecular alterations in the serum, including lipoproteins (APOA2, APOB and APOC1), LCAT, and LysoPCs (Sn-Glycerol 3-phosphoethanolamine; Glycerophosphocholine; Phosphatidylcholine), were mainly associated with the lipid metabolism pathway. Interestingly, as shown in **Fig. 9B**, the cholesterol metabolism and glycerophospholipid metabolism which were two important parts of the lipid metabolism pathway shared one common lipoprotein, LCAT. Previously, a great number of reports had revealed that AS patients with high disease activity was closely related to a deteriorated lipid profile, which suggested that lipid metabolism pathway might be involved in the pathogenesis of AS [71, 72].

Compared with the HC group, proteins associated with cholesterol metabolism including APOA, APOB, APOC1 and LCAT were differently regulated in the AS model group. APOA is a high-density lipoprotein (HDL) apolipoprotein, which can transfer cholesterol from tissues to the liver for decomposition. Importantly, Lecithin cholesterol acyltransferase (LCAT) is the key enzyme in this metabolic process, which can elevate the expression of APOA and further promote the clearance of cholesterol [73]. However, in this study, inflammatory conditions induced by AS decreased capacity of HDL and LCAT to efficiently transfer excess cholesterol in the ligament tissue to the liver, leading to the ectopic fat deposition in the ligaments of AS model mice [74]. Then, ectopic fat deposition could further promote the production of inflammatory cytokines, which resulted in cartilage dysfunction and degeneration in patients with AS. Our previous LC-MS based tissue metabolomics research [22] had shown that moxibustion intervention could correct the abnormal ectopic fat deposition through decreasing the tissue metabolic levels of cholesterol in AS model mice. The results of this multi-omic study further support our previous metabolomic study, suggesting that

moxibustion at specific acupuncture points can ameliorate the ectopic fat deposition of AS by up-regulating the expression levels of APOA and HDL proteins related to cholesterol synthesis and transport.

In contrast, the other two lipoproteins, including APOB and APOC, significantly increased in the AS model mice. These results were in agreement with our previous clinical proteomic study, which showed that APOB and APOC were over-expressed in the serum of AS patients compared with healthy controls [75]. APOB and APOC were the main protein components of low-density lipoproteins (LDL) and very low density lipoproteins (VLDL), respectively, and they were important biomarkers for predicting the cardiovascular (CV) risks [76]. It has been reported that the CV event is the leading cause of mortality in AS, which is partly due to the dyslipidemia in AS patients, including high levels of APOB and APOC [77]. Previously, Huang *et al* [78] reported that plasma levels of APOB and APOC markedly decreased in the hyperlipidemia rabbit model and increased following herbal-partitioned moxibustion. In line with the previous research, in this study, moxibustion may also well have a clinically relevant effect on decreasing the CV risks of AS by down-regulating the serum levels of APOB and APOC.

LysoPCs, the main active components of oxidized low-density lipoprotein (ox-LDL) in the glycerophospholipid metabolism pathway, have been confirmed to be generated by lecithin after being hydrolyzed by LCAT. It was reported that high concentrations of LysoPCs could active neutrophils and macrophage and cause oxidative stress damage in the cell membrane [79]. Previously, moxibustion had exerted a protective effect on cell membrane of rats with ethanol-induced gastric mucosal lesions through down-regulating the serum levels of LysoPCs [31]. Similarity, the levels of three LysoPCs compounds are reversed by moxibustion at GV4, BL23 and ST36, suggesting that moxibustion at specific acupuncture points treatment has the ability to ameliorate the cellular injury in AS.

Purine metabolism

It was reported that the purine metabolism was notably involved in the pathogenesis of adult and pediatric spinal spondyloarthritis, and overproduction of proteins and metabolites in purine metabolism could aggravate joint and cartilage tissue injury for AS patients [80, 81]. Consistent with those previous studies, the up-regulation of XDH and its downstream metabolic products inosine, hypoxanthine, xanthine, xanthosine and uracil in AS model mice in the current study also suggested that AS had critically influenced purine metabolism. XDH is a key rate-limiting enzyme in purine degradation, which contributes to transferring hypoxanthine to xanthine. Inosine and uracil are downstream metabolites of nucleotides through the purine metabolism pathway. Moreover, inosine can also be served as novel small-molecule fecal biomarkers in AS and showed a close relationship with the inflammatory indicator ESR [82]. Previously, methotrexate (MTX), the second line disease modifying antirheumatic drug prescribed in AS patients, exerted anti-inflammatory effects for AS via inhibiting purine metabolism [83]. Moreover, Du *et al* [84] performed the LC-Q/TOF-MS metabolomics approach to discover the effect of heat-reinforcing acupuncture at ST36 on urinary metabolic fingerprinting of arthritis rabbit with cold syndrome. They also found that compared with the model group, the purine metabolism in the heat-reinforcing acupuncture group was significantly decreased. Results of this study exhibited that the molecular levels of XDH, inosine, hypoxanthine, xanthine, xanthosine and uracil in AS mice were markedly down-regulated by acupuncture points' moxibustion therapy, suggesting a similarity of anti-AS mechanisms to MTX and acupuncture.

Glycolysis/gluconeogenesis

Glycolysis/gluconeogenesis, another important metabolic pathway that supplies ATP for organisms, plays a key role in maintaining the energy homeostasis. PGAM1 is an important metabolic enzyme that participates in the glycolysis/gluconeogenesis pathway by interconverting 3- and 2-phosphoglycerate with 2,3-bisphosphoglycerate. It has been reported that the expression levels of the PGAM1 in PBMCs of AS patients are higher than those of healthy volunteers, implying that glycolysis is activated under systemic inflammatory conditions, which further results in a hypoxic microenvironment that induces the chondrocyte apoptosis [85, 86]. However, in this study, moxibustion can ameliorate the hypoxic microenvironment and reduce chondrocyte apoptosis in AS mice via down-regulating the serum levels of PGAM1 that involve in the glycolysis/gluconeogenesis pathway, which is in agreement with our previous studies [22, 32]. Moreover, PGAM1 changes were also closely related to the improvement of pathological results of cartilage tissue (**Additional file 1: Figure S1**) and the decrease of AI score in the MA group (**Fig. 2A**).

Glucose 6-phosphate, D-Mannose and ethanoic acid, the downstream metabolites of PGAM1, were all markedly up-regulated in the AS model mice, which was in line with our proteomic study and further supported the enhancing activity of glycolysis and dysfunction of energy metabolism in AS. Our previous urinary metabolomic study [22] had revealed that metabolites that were involved in glycolysis/gluconeogenesis were all significantly down-regulated following moxibustion intervention. In this study, moxibustion may correct the impairment of energy metabolism through decreasing the serum levels of Glucose 6-phosphate, D-Mannose and ethanoic acid, which was somewhat in line with the previous research.

Glycine, serine and threonine metabolism

The altered proteins and metabolites involved in the glycine serine and threonine metabolism has been reported in PBMCs isolated from the plasma of AS patients [85] and the fecal extracts of AS modeling rats [87]. These past findings are consistent with our current results.

Notably, PGAM1 is not only involved in glycolysis/gluconeogenesis but also simultaneously participates in glycine, serine and threonine metabolism. PGAM1 has a lot of subfamily protein members, including Bisphosphoglycerate Mutase (BPGM), which can control glycolytic intermediate levels and further modulate the serine synthesis. Thus, the up-regulation of serine concentration caused by the increasing of PGAM1 levels in glycolysis/gluconeogenesis pathway can result in the misfolding of the HLA-B27 protein process, which plays an important role in the pathogenesis of AS [88]. However, the protein level of PGAM1 together with the metabolic concentration of serine in the moxibustion at acupuncture points group are lower than that in the AS model group, which suggests that moxibustion can simultaneously improve the energy homeostasis and ammonia acid metabolism.

Glycine, as a decomposition product by serine, has been revealed to possess anti-inflammatory properties [89]. Thus, lower levels of glycine in serum samples of AS model mice and the depletion is reversed by 4-week moxibustion at specific acupuncture points, indicating that AS modeling may cause a weaken anti-inflammatory properties and acupuncture points' moxibustion therapy has a positive effect in improving this trend.

Taurine, as a sulfur-containing AA, plays an important role in directly scavenging reactive oxygen species and protecting joint tissue from oxidative stress in progressive inflammatory diseases [90]. In this research, the serum level of taurine significantly down-regulates in AS model mice suggesting that the dysfunction of taurine and hypotaurine metabolism and decreasing in antioxidant capacity exist during the pathological process of AS. Recently, Zhang *et al* [91] proved that moxibustion at ST36 and BL23 acupuncture points could up-regulate the serum level of taurine in CIA rats. Similarity, the decreasing AI scores and increasing concentration of taurine following moxibustion at specific acupuncture points in this study seemed to be a serum biomarker of the AS model mice in local defense reactions against oxidative stress injury.

Phenylalanine metabolism

During the development of AS, the dysregulation of tight junctions between intestinal epithelial cells increased gut permeability then led to subsequent gut leaky. Pathogenic microbiota from gut leaky of the intestinal epithelium could further result in the dysregulation of osteoproliferation in bone marrow through activating innate immunity system and IL-23/Th17 axis of AS [92]. Interestingly, the Macrophage migration inhibitory factor (MIF) is also mainly involved in the innate immune response of pathogenic microbiota caused by gut leakage. Some specific gut pathogens, including the *Helicobacter pylori*, have been proven to trigger the release of MIF [93]. Subsequently, the production of MIF from the gut may drive the new bone formation in patients with AS via activating and mineralizing OBs, upregulating genes involved in osteogenesis, and triggering the stabilization of β-catenin, an important mediator involved in the OB-specific Wnt/β-catenin pathway [70]. Thus, it is not surprising to detect the high concentration of MIF in patients with AS [94]. Moreover, the serum level of MIF could also independently predict radiographic progression in the spine of AS patients [95]. However, moxibustion may directly decrease the osteogenesis of AS through downregulating the serum levels of MIF, which is in line with the reducing trends of ALP and OCN after moxibustion intervention (**Fig. 10** and **Additional file 1: Figure S7**).

Increased levels of L-Phenylalanine, tyrosine and L-histidine in the AS model group could reflect early changes in colonic protein fermentation and the disturbances of intestinal homeostasis, which may further result in abnormal metabolism of intestinal flora and phenylalanine [87]. The previous study had proved that herbal-partitioned moxibustion could protect the integrity of intestinal barrier in rats with ulcerative colitis by reversing microbiota profiles and rebalancing the intestinal microbial environment [96]. Moreover, our previous research [97] had found that moxibustion at ST36 and BL23 acupuncture points could attenuate inflammatory symptoms of CIA model rats to some extent via decreasing the urine level of L-phenylalanine and tyrosine. In line with previous works, serum levels of L-Phenylalanine, tyrosine and L-histidine are down-regulated after moxibustion intervention at GV4, BL23 and ST36 acupuncture points in AS mice, which indicate that moxibustion can ameliorate the dysbiosis of intestinal flora and the perturbed phenylalanine metabolism pathway in AS.

Limitation

There are several potential limits of this study. Firstly, we only select a single time point to explore the possible molecular mechanism of moxibustion for AS mice. However, the time-relative therapeutic mechanism of moxibustion on AS is still scarce. Secondly, some lipoproteins and LysoPCs were found to be involved in the anti-AS effects of moxibustion based on the DIA-MS based proteomic and UHPLC-Q-TOF/MS based metabolomics. In the future, targeted lipidomics technique is encouraged to further elucidate the possible lipid metabolism mechanism of moxibustion for treating AS. Thirdly, moxibustion may exert anti-AS effect through alleviating the dysbiosis of intestinal flora and the perturbed phenylalanine metabolism pathway. However, considering the complexity of gut microbiota, the intestinal flora mechanism of moxibustion in the treatment of AS can be also further studied in-depth by combining with 16S rDNA gene sequencing and metagenomic sequencing technologies.

Conclusions

In conclusion, moxibustion achieved its anti-AS effect probably by modulating mineral absorption, lipid metabolism, purine metabolism, glycolysis/gluconeogenesis, glycine, serine and threonine metabolism and phenylalanine metabolism pathways at system level. Combing DIA-MS based proteomic and UHPLC-Q-TOF/MS based metabolomics approach, as a promising tool, can advance our understanding of potential mechanisms of action of moxibustion for AS from a holistic perspective.

Abbreviations

AS: ankylosing spondylitis; ASAS: Assessment of SpondyloArthritis international Society; ACR: American College of Rheumatology; AI: arthritis index; ALP: alkaline phosphatase; CRP: C-reactive protein; CIA: collagen-induced arthritis; DDA: dimethyldioctadecylammonium; DIA-MS: data independent acquisition-mass spectrometry; DEPs: differentially expressed proteins; EULAR：European League Against Rheumatism; ELISA: enzyme-linked immunosorbent assay; ESR: erythrocyte sedimentation rate; FDR: False Discovery Rate; HC: healthy control; HRQoL: health-related quality of life; HDL: high-density lipoprotein; IFN-γ: Interferon-γ; IL-17: Interleukin-17; MA: moxibustion at acupuncture points; MNA: moxibustion at non-acupuncture points; NSAIDs: nonsteroidal anti-inflammatory drugs; OCN: osteocalcin; OB: osteoblast; OPLS-DA: orthogonal projection to latent structure-discriminate analysis; QC: quality control; PLS-DA: partial least squares discriminant analysis; PG: proteoglycans; PBMCs: peripheral blood mononuclear cells RCT: reverse cholesterol transport; SpA: spondyloarthropathy; TIC: total ion chromatogram; TCM: traditional Chinese medicine; TIC: total ion chromatogram; UHPLC-Q-TOF/MS: ultra high performance liquid chromatography quadrupole-time of flight mass spectrometry; MVA: multivariate statistical analysis; MetPA: Metabolomics Pathway Analysis; MTX: methotrexate; VIP: variable importance for project

Declarations

Authors' contributions

Xiao Xu: Conceptualization, Data curation, Formal analysis, Funding acquisition, Methodology, Resources, Software, Validation, Visualization, Writing - original draft, and Writing - review & editing. Ting Liu, Rong-Yun Wang and Ya-Nan Shi: Data curation, Formal analysis, Software, Validation, Methodology. Jing-ming Xu, Wen Mao Feng-qin Wu, Hong-yuan Wang and Zhi-Ling Sun: Methodology, Resources. Qiu-Hua Sun: Conceptualization, Investigation, Methodology, Project administration, Resources, Supervision, Funding acquisition, Writing - review & editing

Acknowledgements

We would like to appreciate the editor and all staff working in editorial office of *Chinese Medicine*.

Funding

This study was supported by National Natural Science Foundation of China (No. 81904274, 81973756 and 81774383).

Availability of data and materials

Data will be made available upon request.

Ethics approval and consent to participate

This study has been approved by the ethical review of experimental animal welfare in Zhejiang Chinese Medical University (No. SCXK2016-0010).

Consent for publication

Not applicable.

Competing interests

The authors declare that there is no conflict of interest.

References

1. Braun J, Sieper J: Ankylosing spondylitis. Lancet 2007, 369(9570):1379-1390. doi: 1310.1016/S0140-6736(1307)60635-60637.
2. Campochiaro C, Caruso PF: Ankylosing Spondylitis and Axial Spondyloarthritis. N Engl J Med 2016, 375(13):1302. doi: 1310.1056/NEJMc1609622.
3. Kidd B, Mullee M, Frank A, Cawley M: Disease expression of ankylosing spondylitis in males and females. J Rheumatol 1988, 15(9):1407-1409.
4. Xu X, Shen B, Zhang A, Liu J, Da Z, Liu H, Gu Z: Anxiety and depression correlate with disease and quality-of-life parameters in Chinese patients with ankylosing spondylitis. Patient Prefer Adherence 2016, 10:879-85.(doi):10.2147/PPA.S86612. eCollection 82016.
5. Shen B, Zhang A, Liu J, Da Z, Xu X, Gu Z: A primary analysis of sexual problems in Chinese patients with ankylosing spondylitis. Rheumatol Int 2013, 33(6):1429-1435. doi: 1410.1007/s00296-00012-02565-00293. Epub 02012 Nov 00215.
6. Ward MM, Deodhar A, Akl EA, Lui A, Ermann J, Gensler LS, Smith JA, Borenstein D, Hiratzka J, Weiss PF et al: American College of Rheumatology/Spondylitis Association of America/Spondyloarthritis Research and Treatment Network 2015 Recommendations for the Treatment of Ankylosing Spondylitis and Nonradiographic Axial Spondyloarthritis. Arthritis Rheumatol 2016, 68(2):282-298. doi: 210.1002/art.39298. Epub 32015 Sep 39224.
7. Dougados M, Behier JM, Jolchine I, Calin A, van der Heijde D, Olivieri I, Zeidler H, Herman H: Efficacy of celecoxib, a cyclooxygenase 2-specific inhibitor, in the treatment of ankylosing spondylitis: a six-week controlled study with comparison against placebo and against a conventional nonsteroidal antiinflammatory drug. Arthritis Rheum 2001, 44(1):180-185. doi: 110.1002/1529-0131(200101)200144:200101<200180::AID-ANR200124>200103.200100.CO;200102-K.
8. Mansour M, Cheema GS, Naguwa SM, Greenspan A, Borchers AT, Keen CL, Gershwin ME: Ankylosing spondylitis: a contemporary perspective on diagnosis and treatment. Semin Arthritis Rheum 2007, 36(4):210-223. doi: 210.1016/j.semarthrit.2006.1008.1003. Epub 2006 Sep 1029.
9. Sieper J, Poddubnyy D: New evidence on the management of spondyloarthritis. Nat Rev Rheumatol 2016, 12(5):282-295. doi: 210.1038/nrrheum.2016.1042. Epub 2016 Apr 1037.
10. Chen LT, Chen YF: Pharmacoeconomic analysis of biological agents in the treatment of ankylosing spondylitis. Chin J Pharma Economic 2016, 11(5):7-10.
11. Wang ZZ: Research progress of traditional Chinese medicine nursing for ankylosing spondylitis. Rheumatol and Arthritis 2019, 8(7):77-80.
12. Xu X, Chen Z, Wang H-Y, Li L, Lu J, Yan M, Ding C-Y, Sun Z-Q, Sun Q-H: Moxibustion intervention for patients with ankylosing spondylitis: A study for a pilot randomized controlled trial. Eur J Integra Med 2019, 27:18-26.
13. Wang H-Y, Xu X, Li L, Ding C-Y, Lu J, Zhang Y-y, Zhang Y-f, Zhang Y-l, Sun Z-Q: Moxibustion therapy in Chinese patients with ankylosing spondylitis: A randomized controlled pilot trial. Eur J Integra Med 2019, 31:100952.
14. Xu X, Cao L, Mwandalima CJ, Wang Z, Liu L, Sun Z-Q: Systematic review and meta-analysis: Moxibustion for treating ankylosing spondylitis. Eur J Integra Med 2017, 12:142-146.

15. Zhang T, Liu W, Ma HH: Clinical study on the treatment of ankylosing spondylitis by Moxibustion. Shandong J TCM 2013, 32(12):897-900.
16. Gao D, Wang YY, Yao JS: Clinical research progress of Moxibustion in the treatment of ankylosing spondylitis. Rheumatol and Arthritis 2016, 5(5):61-64.
17. Robinson, Nicola, Liu, Jianping, Witt, Claudia, M.: Combining 'omics and comparative effectiveness research: Evidence-based clinical research decision-making for Chinese medicine. Science 2015, 347(6219):S50-S51.
18. van der Greef J: Perspective: All systems go. Nature 2011, 480(7378):S87. doi: 10.1038/1480S1087a.
19. Zhang A, Sun H, Yan G, Cheng W, Wang X: Systems biology approach opens door to essence of acupuncture. Complement Ther Med 2013, 21(3):253-259. doi: 210.1016/j.ctim.2013.1003.1002. Epub 2013 Mar 1025.
20. Johnson CH, Ivanisevic J, Siuzdak G: Metabolomics: beyond biomarkers and towards mechanisms. Nat Rev Mol Cell Biol 2016, 17(7):451-459. doi: 410.1038/nrm.2016.1025. Epub 2016 Mar 1016.
21. Casadei L, Valerio M, Manetti C: Metabolomics: Challenges and Opportunities in Systems Biology Studies. Methods Mol Biol 2018, 1702:327-336. (doi):10.1007/1978-1001-4939-7456-1006_1016.
22. Xu X, Shi Y-N, Wang R-Y, Ding C-Y, Zhou X, Zhang Y-F, Sun Z-L, Sun Z-Q, Sun Q-H: Metabolomic analysis of biochemical changes in the tissue and urine of proteoglycan-induced spondylitis in mice after treatment with moxibustion. Integr Med Res 2020:100428.
23. Misra B: Individualized metabolomics: opportunities and challenges. Clin Chem Lab Med 2020, 58(6):939-947. doi: 910.1515/cclm-2019-0130.
24. Gioria S, Lobo Vicente J, Barboro P, La Spina R, Tomasi G, Urbán P, Kinsner-Ovaskainen A, François R, Chassaigne H: A combined proteomics and metabolomics approach to assess the effects of gold nanoparticles in vitro. Nanotoxicology 2016, 10(6):736-748. doi: 710.3109/17435390.17432015.11121412. Epub 17432016 Feb 17435310.
25. Song YN, Dong S, Wei B, Liu P, Zhang YY, Su SB: Metabolomic mechanisms of gypenoside against liver fibrosis in rats: An integrative analysis of proteomics and metabolomics data. PLoS One 2017, 12(3):e0173598. doi: 0173510.0171371/journal.pone.0173598. eCollection 0172017.
26. Xu Y, Dou D, Ran X, Liu C, Chen J: Integrative analysis of proteomics and metabolomics of anaphylactoid reaction induced by Xuesaitong injection. J Chromatogr A 2015, 1416:103-11.(doi):10.1016/j.chroma.2015.1009.1019. Epub 2015 Sep 1018.
27. Walsh MC, Brennan L, Malthouse JP, Roche HM, Gibney MJ: Effect of acute dietary standardization on the urinary, plasma, and salivary metabolomic profiles of healthy humans. Am J Clin Nutr 2006, 84(3):531-539. doi: 510.1093/ajcn/1084.1093.1531.
28. Bardos T, Szabo Z, Czipri M, Vermes C, Tunyogi-Csapo M, Urban RM, Mikecz K, Glant TT: A longitudinal study on an autoimmune murine model of ankylosing spondylitis. Ann Rheum Dis 2005, 64(7):981-987. doi: 910.1136/ard.2004.029710. Epub 022005 Jan 029717.
29. Ishikawa LL, Colavite PM, da Rosa LC, Balbino B, Franca TG, Zorzella-Pezavento SF, Chiuso-Minicucci F, Sartori A: Commercial bovine proteoglycan is highly arthritogenic and can be used as an alternative antigen source for PGIA model. Biomed Res Int 2014, 2014:148594.(doi):10.1155/2014/148594. Epub 142014 May 148527.
30. Li J, Li H, Zhang J: A proteoglycan-induced spondyloarthritis mouse model and the therapeutic effect of CCN1 monoclonal antibody. Chin J Rheumatol 2019, 23(8):513-517.
31. Zhang Y, Huang MS, Liu CC, Lian LY, Shen JC, He QD, Wang YJ, Zhang LB, Liu M, Yang ZB: Dynamic observation and analysis of metabolic response to moxibustion stimulation on ethanol-induced gastric mucosal lesions (GML) rats. Chin Med 2019, 14:44.(doi):10.1186/s13020-13019-10266-13025. eCollection 12019.
32. Xu X, Wang MM, Sun ZL, Zhou DP, Wang L, Wang FQ, Xu ZY, Ma Q: Discovery of serum proteomic biomarkers for prediction of response to moxibustion treatment in rats with collagen-induced arthritis: an exploratory analysis. Acupunct Med 2016, 34(3):184-193. doi: 110.1136/acupmed-2015-010909. Epub 012015 Nov 010905.
33. Z.R. L: Experimental Acupuncture & Moxibustion. Beijing: China: Press of Traditional Chinese Medicine; 2003.
34. Lee B, Sur B, Shim J, Hahm DH, Lee H: Acupuncture stimulation improves scopolamine-induced cognitive impairment via activation of cholinergic system and regulation of BDNF and CREB expressions in rats. BMC Complement Altern Med 2014, 14:338.(doi):10.1186/1472-6882-1114-1338.
35. Huang Y, Lu SF, Hu CJ, Fu SP, Shen WX, Liu WX, Li Q, Wang N, He SY, Liang FR et al: Electro-acupuncture at Neiguan pretreatment alters genome-wide gene expressions and protects rat myocardium against ischemia-reperfusion. Molecules 2014, 19(10):16158-16178. doi: 16110.13390/molecules191016158.
36. Tautenhahn R, Patti GJ, Rinehart D, Siuzdak G: XCMS Online: a web-based platform to process untargeted metabolomic data. Anal Chem 2012, 84(11):5035-5039. doi: 5010.1021/ac300698c. Epub 302012 May 300610.
37. Chong J, Soufan O, Li C, Caraus I, Li S, Bourque G, Wishart DS, Xia J: MetaboAnalyst 4.0: towards more transparent and integrative metabolomics analysis. Nucleic Acids Res 2018, 46(W1):W486-W494. doi: 410.1093/nar/gky1310.
38. Xu J, Lin X, Cheng KK, Zhong H, Liu M, Zhang G, Shen G, Dong J: Metabolic Response in Rats following Electroacupuncture or Moxibustion Stimulation. Evid Based Complement Alternat Med 2019, 2019:6947471.(doi):10.1155/2019/6947471. eCollection 6942019.
39. Lin X, Liu X, Xu J, Cheng KK, Cao J, Liu T, Liu Q, Zhong H, Shen G, Dong J et al: Metabolomics analysis of herb-partitioned moxibustion treatment on rats with diarrhea-predominant irritable bowel syndrome. Chin Med 2019, 14:18.(doi):10.1186/s13020-13019-10240-13022. eCollection 12019.
40. Wiśniewski JR, Zougman A, Nagaraj N, Mann M: Universal sample preparation method for proteome analysis. Nat Methods 2009, 6(5):359-362. doi: 310.1038/nmeth.1322. Epub 2009 Apr 1019.
41. Han D, Jin J, Woo J, Min H, Kim Y: Proteomic analysis of mouse astrocytes and their secretome by a combination of FASP and StageTip-based, high pH, reversed-phase fractionation. Proteomics 2014, 14(13-14):1604-1609. doi: 1610.1002/pmic.201300495. Epub 201302014 May 201300428.
42. Shi J, Wang X, Lyu L, Jiang H, Zhu HJ: Comparison of protein expression between human livers and the hepatic cell lines HepG2, Hep3B, and Huh7 using SWATH and MRM-HR proteomics: Focusing on drug-metabolizing enzymes. Drug Metab Pharmacokinet 2018, 33(2):133-140. doi: 110.1016/j.dmpk.2018.1003.1003. Epub 2018 Mar 1010.

43. Maere S, Heymans K, Kuiper M: BiNGO: a Cytoscape plugin to assess overrepresentation of gene ontology categories in biological networks. Bioinformatics 2005, 21(16):3448-3449. doi: 3410.1093/bioinformatics/bti3551. Epub 2005 Jun 3421.
44. Zhao DS, Jiang LL, Wang LL, Wu ZT, Li ZQ, Shi W, Li P, Jiang Y, Li HJ: Integrated Metabolomics and Proteomics Approach To Identify Metabolic Abnormalities in Rats with Dioscorea bulbifera Rhizome-Induced Hepatotoxicity. Chem Res Toxicol 2018, 31(9):843-851. doi: 810.1021/acs.chemrestox.1028b00066. Epub 02018 Aug 00010.
45. Basu S, Duren W, Evans CR, Burant CF, Michailidis G, Karnovsky A: Sparse network modeling and metscape-based visualization methods for the analysis of large-scale metabolomics data. Bioinformatics 2017, 33(10):1545-1553. doi: 1510.1093/bioinformatics/btx1012.
46. Gika HG, Theodoridis GA, Wingate JE, Wilson ID: Within-day reproducibility of an HPLC-MS-based method for metabonomic analysis: application to human urine. J Proteome Res 2007, 6(8):3291-3303. doi: 3210.1021/pr070183p. Epub 072007 Jul 070111.
47. Lundstedt T, Seifert E, Abramo L, Thelin B, Nyström Å, Pettersen J, Bergman R: Experimental design and optimization. Chemometrics and Intelligent Laboratory Systems 1998, 42(1):3-40.
48. Cai A, Qi S, Su Z, Shen H, Yang Y, He L, Dai Y: Quantitative Proteomic Analysis of Peripheral Blood Mononuclear Cells in Ankylosing Spondylitis by iTRAQ. Clin Transl Sci 2015, 8(5):579-583. doi: 510.1111/cts.12265. Epub 12015 Mar 12219.
49. Niccoli L, Nannini C, Cassarà E, Kaloudi O, Cantini F: Frequency of anemia of inflammation in patients with ankylosing spondylitis requiring anti-TNFα drugs and therapy-induced changes. Int J Rheum Dis 2012, 15(1):56-61. doi: 10.1111/j.1756-1185X.2011.01662.x. Epub 02011 Sep 01614.
50. Li Y, Bai B, Zhang Y: Expression of iron-regulators in the bone tissue of rats with and without iron overload. Biometals 2018, 31(5):749-757. doi: 710.1007/s10534-10018-10133-10533. Epub 12018 Jul 10519.
51. Yamasaki K, Hagiwara H: Excess iron inhibits osteoblast metabolism. Toxicol Lett 2009, 191(2-3):211-215. doi: 210.1016/j.toxlet.2009.1008.1023. Epub 2009 Sep 1016.
52. Schett G: Bone formation versus bone resorption in ankylosing spondylitis. Adv Exp Med Biol 2009, 649:114-21.(doi):10.1007/1978-1001-4419-0298-1006_1008.
53. Grisar J, Bernecker PM, Aringer M, Redlich K, Sedlak M, Wolozcszuk W, Spitzauer S, Grampp S, Kainberger F, Ebner W et al: Ankylosing spondylitis, psoriatic arthritis, and reactive arthritis show increased bone resorption, but differ with regard to bone formation. J Rheumatol 2002, 29(7):1430-1436.
54. Li T, Huang Z, Zheng B, Liao Z, Zhao L, Gu J: Serum disease-associated proteins of ankylosing spondylitis: results of a preliminary study by comparative proteomics. Clin Exp Rheumatol 2010, 28(2):201-207. Epub 2010 May 2013.
55. Yildirim K, Erdal A, Karatay S, Melikoğlu MA, Uğur M, Senel K: Relationship between some acute phase reactants and the Bath Ankylosing Spondylitis Disease Activity Index in patients with ankylosing spondylitis. South Med J 2004, 97(4):350-353. doi: 310.1097/1001.SMJ.0000066946.0000056322.0000066943C.
56. Gundogdu M, Kaya H, Gulcin I, Erdem F, Cayir K, Keles M, Yilmaz A: Oxidase activity of ceruloplasmin and some acute phase reactant and trace element concentrations in serum of patients with chronic lymphocytic leukemia. Scott Med J 2007, 52(1):24-27. doi: 10.1258/rsmsmj.1252.1251.1224.
57. Surrall KE, Bird HA, Dixon JS: Caeruloplasmin, prealbumin and alpha 2-macroglobulin as potential indices of disease activity in different arthritides. Clin Rheumatol 1987, 6(1):64-69. doi: 10.1007/BF02201003.
58. Mackiewicz A, Khan MA, Reynolds TL, van der Linden S, Kushner I: Serum IgA, acute phase proteins, and glycosylation of alpha 1-acid glycoprotein in ankylosing spondylitis. Ann Rheum Dis 1989, 48(2):99-103. doi: 110.1136/ard.1148.1132.1199.
59. Shi .Jia L, Wei J: Application of three serum proteins in the diagnosis of ankylosing spondylitis. . In.; 2019.
60. Tolosano E, Altruda F: Hemopexin: structure, function, and regulation. DNA Cell Biol 2002, 21(4):297-306. doi: 210.1089/104454902753759717.
61. Lee YS, Kim AY, Choi JW, Kim M, Yasue S, Son HJ, Masuzaki H, Park KS, Kim JB: Dysregulation of adipose glutathione peroxidase 3 in obesity contributes to local and systemic oxidative stress. Mol Endocrinol 2008, 22(9):2176-2189. doi: 2110.1210/me.2008-0023. Epub 2008 Jun 2118.
62. Jiang X, Sun Z, Zhou D, Xu X: Effect of moxibustion on synovial lesions of rheumatoid arthritis rats. Chin J Gerontol 2015, 35(19):5386-5389.
63. Srivastava P: Roles of heat-shock proteins in innate and adaptive immunity. Nat Rev Immunol 2002, 2(3):185-194. doi: 110.1038/nri1749.
64. Cakmak YO: A review of the potential effect of electroacupuncture and moxibustion on cell repair and survival: the role of heat shock proteins. Acupunct Med 2009, 27(4):183-186. doi: 110.1136/aim.2009.001420.
65. Yi SX, Peng Y, Chang XR, Peng N, Yan J, Lin YP: Effect of pre-moxibustion on apoptosis and proliferation of gastric mucosa cells. World J Gastroenterol 2007, 13(15):2174-2178. doi: 2110.3748/wjg.v2113.i2115.2174.
66. Chang XR, Peng L, Yi SX, Peng Y, Yan J: Association of high expression in rat gastric mucosal heat shock protein 70 induced by moxibustion pretreatment with protection against stress injury. World J Gastroenterol 2007, 13(32):4355-4359. doi: 4310.3748/wjg.v4313.i4332.4355.
67. Wright C, Edelmann M, diGleria K, Kollnberger S, Kramer H, McGowan S, McHugh K, Taylor S, Kessler B, Bowness P: Ankylosing spondylitis monocytes show upregulation of proteins involved in inflammation and the ubiquitin proteasome pathway. Ann Rheum Dis 2009, 68(10):1626-1632. doi: 1610.1136/ard.2008.097204. Epub 092008 Oct 097224.
68. Murata S, Takahama Y, Kasahara M, Tanaka K: The immunoproteasome and thymoproteasome: functions, evolution and human disease. Nat Immunol 2018, 19(9):923-931. doi: 910.1038/s41590-41018-40186-z. Epub 42018 Aug 41513.
69. Alvarez I, Sesma L, Marcilla M, Ramos M, Marti M, Camafeita E, de Castro JA: Identification of novel HLA-B27 ligands derived from polymorphic regions of its own or other class I molecules based on direct generation by 20 S proteasome. J Biol Chem 2001, 276(35):32729-32737. doi: 32710.31074/jbc.M104663200. Epub 104662001 Jul 104663202.
70. Maksymowych WP: Biomarkers for Diagnosis of Axial Spondyloarthritis, Disease Activity, Prognosis, and Prediction of Response to Therapy. Front Immunol 2019, 10:305.(doi):10.3389/fimmu.2019.00305. eCollection 02019.

71. van Halm VP, van Denderen JC, Peters MJ, Twisk JW, van der Paardt M, van der Horst-Bruinsma IE, van de Stadt RJ, de Koning MH, Dijkmans BA, Nurmohamed MT: Increased disease activity is associated with a deteriorated lipid profile in patients with ankylosing spondylitis. Ann Rheum Dis 2006, 65(11):1473-1477. doi: 1410.1136/ard.2005.050443. Epub 052006 Apr 050427.
72. van Eijk IC, de Vries MK, Levels JH, Peters MJ, Huizer EE, Dijkmans BA, van der Horst-Bruinsma IE, Hazenberg BP, van de Stadt RJ, Wolbink GJ et al: Improvement of lipid profile is accompanied by atheroprotective alterations in high-density lipoprotein composition upon tumor necrosis factor blockade: a prospective cohort study in ankylosing spondylitis. Arthritis Rheum 2009, 60(5):1324-1330. doi: 1310.1002/art.24492.
73. Zannis VI, Chroni A, Krieger M: Role of apoA-I, ABCA1, LCAT, and SR-BI in the biogenesis of HDL. J Mol Med (Berl) 2006, 84(4):276-294. doi: 210.1007/s00109-00005-00030-00104. Epub 02006 Feb 00125.
74. Chen R, Han S, Dong D, Wang Y, Liu Q, Xie W, Li M, Yao M: Serum fatty acid profiles and potential biomarkers of ankylosing spondylitis determined by gas chromatography-mass spectrometry and multivariate statistical analysis. Biomed Chromatogr 2015, 29(4):604-611. doi: 610.1002/bmc.3321. Epub 2014 Sep 1015.
75. Sun ZL, Wang MM, Xu X: Study on Serum Proteomics of Rheumatism with Damp-heat Syndrome Based on iTRAQ Labeling Method Combined with Bioinfor-matics Technology. J Nanjing Univ Tradit Chin Med 2016, 32(4):316-321.
76. Sierra-Johnson J, Fisher RM, Romero-Corral A, Somers VK, Lopez-Jimenez F, Ohrvik J, Walldius G, Hellenius ML, Hamsten A: Concentration of apolipoprotein B is comparable with the apolipoprotein B/apolipoprotein A-I ratio and better than routine clinical lipid measurements in predicting coronary heart disease mortality: findings from a multi-ethnic US population. Eur Heart J 2009, 30(6):710-717. doi: 710.1093/eurheartj/ehn1347. Epub 2008 Aug 1091.
77. Moltó A, Nikiphorou E: Comorbidities in Spondyloarthritis. Front Med (Lausanne) 2018, 5:62.(doi):10.3389/fmed.2018.00062. eCollection 02018.
78. Huang WT: Effect of herbal-partitioned moxibustion on blood lipid in hyperlipidemia rabbits. Hunan, China: Hunan University of Chinese Medicine; 2018.
79. Hansen HS, Moesgaard B, Hansen HH, Petersen G: N-Acylethanolamines and precursor phospholipids - relation to cell injury. Chem Phys Lipids 2000, 108(1-2):135-150. doi: 110.1016/s0009-3084(1000)00192-00194.
80. Stoll ML, Kumar R, Lefkowitz EJ, Cron RQ, Morrow CD, Barnes S: Fecal metabolomics in pediatric spondyloarthritis implicate decreased metabolic diversity and altered tryptophan metabolism as pathogenic factors. Genes Immun 2016, 17(7):400-405. doi: 410.1038/gene.2016.1038. Epub 2016 Oct 1027.
81. Jimenez Balderas FJ, Robles EJ, Juan L, Badui E, Arellano H, Espinosa Said L, Mintz Spiro G: Purine metabolism in ankylosing spondylitis: clinical study. Arch Invest Med (Mex) 1989, 20(2):163-170.
82. Shao T-j, He Z-x, Xie Z-j, Li H-c, Wang M-j, Wen C-p: Characterization of ankylosing spondylitis and rheumatoid arthritis using 1H NMR-based metabolomics of human fecal extracts. Metabolomics 2016, 12(4):70.
83. Riksen NP, Barrera P, van den Broek PH, van Riel PL, Smits P, Rongen GA: Methotrexate modulates the kinetics of adenosine in humans in vivo. Ann Rheum Dis 2006, 65(4):465-470. doi: 410.1136/ard.2005.048637. Epub 042005 Nov 048624.
84. Du X, Yuan B, Wang J, Zhang X, Tian L, Ren C, Zeng H: Effects of heat-reinforcing acupuncture on urine metabolites in rheumatoid arthritis rabbits. Zhongguo Zhen Jiu 2017, 37(1):55-60. doi: 10.13703/j.10255-12930.12017.13701.13014.
85. Cai AJ: Proteome and microRNA of peripheral blood mononuclear cells in patients with ankylosing spondylitis. Chongqin, China: Chongqin Medical University; 2013.
86. Song J, Baek IJ, Chun CH, Jin EJ: Dysregulation of the NUDT7-PGAM1 axis is responsible for chondrocyte death during osteoarthritis pathogenesis. Nat Commun 2018, 9(1):3427. doi: 3410.1038/s41467-41018-05787-41460.
87. Asquith M, Davin S, Stauffer P, Michell C, Janowitz C, Lin P, Ensign-Lewis J, Kinchen JM, Koop DR, Rosenbaum JT: Intestinal Metabolites Are Profoundly Altered in the Context of HLA-B27 Expression and Functionally Modulate Disease in a Rat Model of Spondyloarthritis. Arthritis & Rheumatol (Hoboken, NJ) 2017, 69(10):1984-1995.
88. Ruuska M, Sahlberg AS, Colbert RA, Granfors K, Penttinen MA: Enhanced phosphorylation of STAT-1 is dependent on double-stranded RNA-dependent protein kinase signaling in HLA-B27-expressing U937 monocytic cells. Arthritis Rheum 2012, 64(3):772-777. doi: 710.1002/art.33391.
89. Razak MA, Begum PS, Viswanath B, Rajagopal S: Multifarious Beneficial Effect of Nonessential Amino Acid, Glycine: A Review. Oxid Med Cell Longev 2017, 2017:1716701.(doi):10.1155/2017/1716701. Epub 1712017 Mar 1716701.
90. Marcinkiewicz J, Kontny E: Taurine and inflammatory diseases. Amino Acids 2014, 46(1):7-20. doi: 10.1007/s00726-00012-01361-00724. Epub 02012 Jul 00719.
91. Zhang YY: Study on mechanism of collagen-induced arthritis rats treated with moxibustion based on metabonomics. . Nanjing China: Nanjing University of Chinese Medicine; 2018.
92. Yang L, Wang L, Wang X, Xian CJ, Lu H: A Possible Role of Intestinal Microbiota in the Pathogenesis of Ankylosing Spondylitis. Int J Mol Sci 2016, 17(12):2126. doi: 2110.3390/ijms17122126.
93. Xia HH, Lam SK, Chan AO, Lin MC, Kung HF, Ogura K, Berg DE, Wong BC: Macrophage migration inhibitory factor stimulated by Helicobacter pylori increases proliferation of gastric epithelial cells. World J Gastroenterol 2005, 11(13):1946-1950. doi: 1910.3748/wjg.v1911.i1913.1946.
94. Kozaci LD, Sari I, Alacacioglu A, Akar S, Akkoc N: Evaluation of inflammation and oxidative stress in ankylosing spondylitis: a role for macrophage migration inhibitory factor. Mod Rheumatol 2010, 20(1):34-39. doi: 10.1007/s10165-10009-10230-10169. Epub 12009 Sep 10129.
95. Ranganathan V, Ciccia F, Zeng F, Sari I, Guggino G, Muralitharan J, Gracey E, Haroon N: Macrophage Migration Inhibitory Factor Induces Inflammation and Predicts Spinal Progression in Ankylosing Spondylitis. Arthritis Rheumatol 2017, 69(9):1796-1806. doi: 1710.1002/art.40175. Epub 42017 Aug 40113.

96. Ji R, Wang A, Shang H, Chen L, Bao C, Wu L, Wu H, Shi Y: Herb-partitioned moxibustion upregulated the expression of colonic epithelial tight junction-related proteins in Crohn's disease model rats. Chin Med 2016, 11:20.(doi):10.1186/s13020-13016-10090-13020. eCollection 12016.

97. He J: Study on mechanism of collagen-induced arthritis (CIA) rats treated with moxibustion based on urinary metabolomics. Nanjing, China: Nanjing University of Chinese Medicine; 2019.

Tables

Table 1
Potential biomarkers and their metabolic pathways.

Ionization mode/ No	Identification	Formula	HMDB match	Mass (m/z)	R.T. (min)	VIP	Regulation			Related pathway
							AS*	MA#	MNA#–	
ESI+										
1	N-Methylhydantoin	$C_4H_6N_2O_2$	HMDB0003646	115.05	162.68	1.90	↑	↓	–	Arginine and proline metabolism
2	Xanthine	$C_5H_4N_4O_2$	HMDB0000292	153.04	205.58	7.91	↑	↓	–	Purine metabolism
3	Hypoxanthine	$C_5H_4N_4O$	HMDB0000157	137.04	258.631	2.30	↑	↓	–	Purine metabolism
4	Inosine	$C_{10}H_{12}N_4O_5$	HMDB0000195	269.09	212.00	7.72	↑	↓	–	Purine metabolism
5	Phosphorylcholine	$C_5H_{15}NO_4P$	HMDB0001565	184.07	495.65	2.70	↑	↓	↓	Glycerophospholipid metabolism
6	Glucose 6-phosphate	$C_6H_{13}O9_P$	HMDB0001401	261.04	470.483	1.01	↑	↓	↓	Glycolysis/Gluconeoger
7	Taurine	$C_2H_7NO_3S$	HMDB0000251	126.02	205.97	1.33	↓	↑	–	Glycine, serine and threonine metabolism
8	L-Phenylalanine	$C_9H_{11}NO_2$	HMDB0000159	166.09	254.44	3.33	↑	↓	↓	Phenylalanine metaboli
9	12-KETE	$C_{20}H_{30}O_3$	HMDB0013633	319.23	44.73	1.89	↑	↓	–	Arachidonic acid metabolism
10	Tyrosine	$C_9H_{11}NO_3$	HMDB0000158	328.14	298.57	3.80	↑	↓	–	Phenylalanine metaboli
11	Glycerophosphocholine	$C_8H_{21}NO_6P$	HMDB0000086	258.11	383.33	11.41	↑	↓	–	Glycerophospholipid metabolism
12	L-Histidine	$C_6H_9N_3O_2$	HMDB0000177	414.25	156.08	5.57	↑	↓	–	Phenylalanine metaboli
ESI-										
13	Allantoin	$C_4H_6N_4O_3$	HMDB0000462	139.03	300.15	3.98	↑	↓	↓	Purine metabolism
14	Serine	$C_3H_7NO_3$	HMDB0000187	258.04	470.73	1.02	↑	↓	↓	Glycine, serine and threonine metabolism
15	Ethanoic acid	$C_{10}H_9NO_3$	HMDB0000763	190.05	204.40	1.91	↑	↓	↓	Glycolysis/Gluconeoger
16	Sn-Glycerol 3-phosphoethanolamine	$C_6H_{13}NO_7PR$	METPA0497	214.05	389.95	2.21	↑	↓	–	Glycerophospholipid metabolism
17	D-Mannose	$C_6H_{12}O_6$	HMDB0000169	259.02	473.46	2.41	↑	↓	↓	Glycolysis/Gluconeoger
18	Uracil	$C_4H_4N_2O_2$	HMDB0000300	111.02	83.23	4.06	↑	↓	–	Purine metabolism
19	L-Malic acid	$C_4H_6O_5$	HMDB0000156	133.01	401.47	2.42	↑	↓	↓	TCA cycle
20	Glycine	$C_2H_5NO_2$	HMDB0000123	206.08	165.40	1.16	↓	↑	–	Glycine, serine and threonine metabolism
21	Citrate	$C_6H_8O_7$	HMDB0000094	191.02	502.02	6.25	↑	↓	↓	TCA cycle

HC: healthy control group; AS: untreated ankylosing spondylitis group; MA: moxibustion at acupuncture points; MNA: moxibustion at non-acupuncture points R.T.: Retention Time; VIP: Variable importance in the projection

*Compared with the HC group, $*p < 0.05$. #Compared with the AS group, $^{\#}p < 0.05$

Differential metabolites: (↓) down-regulated, (↑) up-regulated, and (–) no significant change.

Table 2
Lists of 21 moxibustion-specific differentially expressed proteins in AS.

No	UniProt accession code	Protein name	Gene symbol	C score	Sequence number	Fold Change		
						AS*	MA#	MNA#
1	P17563	Methanethiol oxidase	Selenbp1	1.028	10	0.277 ↓	3.770 ↑	–
2	P11276	Fibronectin	Fn1	1.114	127	1.430↑	2.160 ↑	–
3	O70435	Proteasome subunit alpha type-3	Psma3	1.092	8	2.161 ↑	0.450 ↓	0.675 ↓
4	Q61646	Haptoglobin	Hp	1.106	44	2.100 ↑	0.097 ↓	–
5	E9Q414	Apolipoprotein B-100	Apob	1.113	116	1.336 ↑	0.766 ↓	0.767 ↓
6	Q9QUM9	Proteasome subunit alpha type-6	Psma6	1.101	10	3.531 ↑	0.320 ↓	–
7	P16301	Phosphatidylcholine-sterol acyltransferase	Lcat	1.099	16	0.709 ↓	1.863 ↑	–
8	Q9R1P3	Proteasome subunit beta type-2	Psmb2	1.081	7	6.106 ↑	0.156 ↓	–
9	Q00519	Xanthine dehydrogenase/oxidase	Xdh	1.028	12	3.369 ↑	0.468 ↓	0.519 ↓
10	Q921I1	Serotransferrin	Tf	1.108	56	1.979 ↑	0.572 ↓	–
11	P21614	Vitamin D-binding protein	Gc	1.106	68	0.728 ↓	1.364 ↑	–
12	Q91 × 72	Hemopexin	Hpx	1.111	66	1.786 ↑	1.353 ↑	–
13	Q9DBJ1	Phosphoglycerate mutase 1	Pgam1	1.074	6	1.781 ↑	0.467 ↓	0.655 ↓
14	P34884	Macrophage migration inhibitory factor	Mif	1.063	4	1.524 ↑	0.753 ↓	–
15	Q61147	Ceruloplasmin	Cp	1.114	124	1.424 ↑	0.767 ↓	–
16	Q60590	Alpha-1-acid glycoprotein 1	Orm1	1.104	17	1.494 ↑	0.621 ↓	–
17	P34928	Apolipoprotein C-I	Apoc1	1.093	17	1.936 ↑	0.733 ↓	–
18	P63017	Heat shock cognate 71 kDa protein	Hspa8	1.098	29	1.830 ↑	1.707 ↑	–
19	P12246	Serum amyloid P-component	Apcs	1.108	11	1.445 ↑	0.462 ↓	–
20	Q01853	Transitional endoplasmic reticulum ATPase	Vcp	1.089	21	1.638 ↑	0.768 ↓	–
21	P09813	Apolipoprotein A-II	Apoa2	1.101	9	0.439 ↓	2.306 ↑	–

HC: healthy control group; AS: untreated ankylosing spondylitis group; MA: moxibustion at acupuncture points; MNA: moxibustion at non-acupuncture points.

*Compared with the HC group, $*p < 0.05$. #Compared with the AS group, $^{\#}p < 0.05$

Differential proteins: (↓) down-regulated, (↑) up-regulated, and (–) no significant change.

Figures

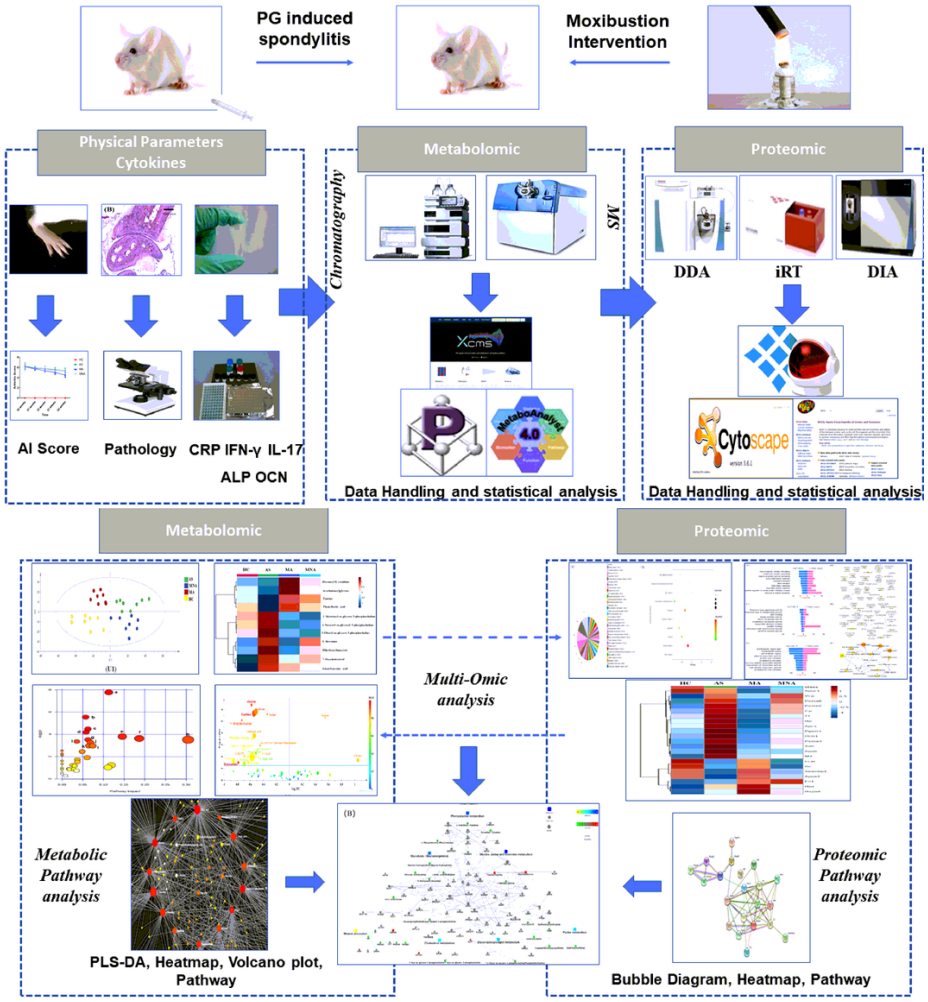

Figure 1

The schematic diagram of the experimental processes.

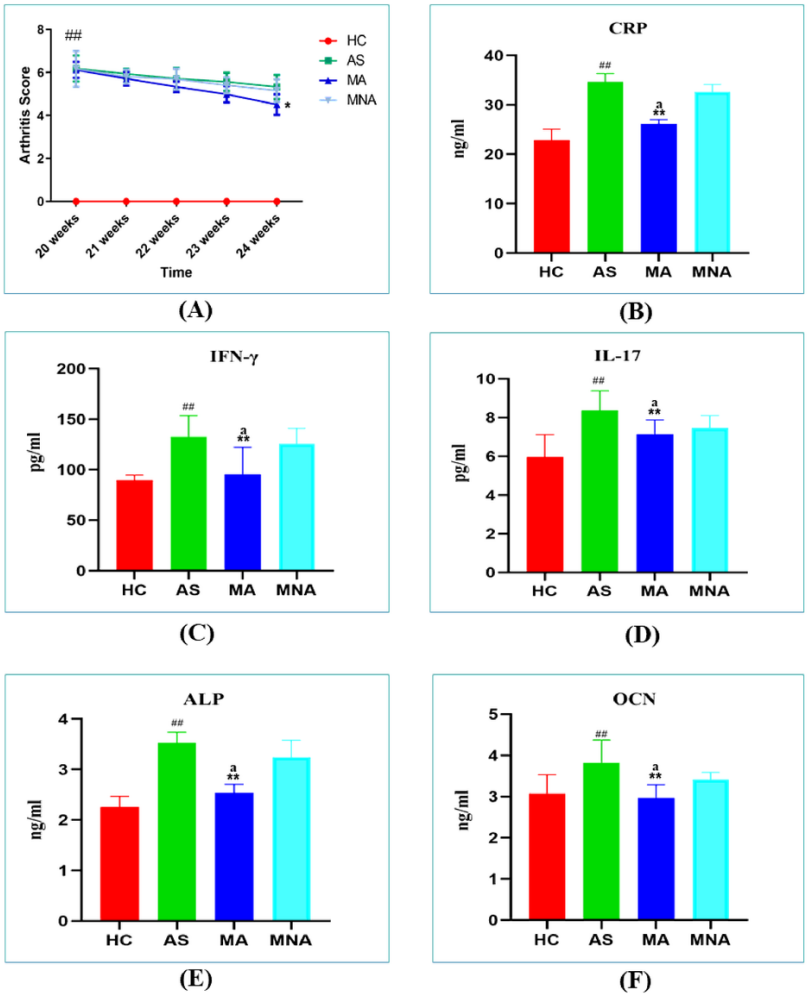

Figure 2

(A) Arthritis index (AI) score from the healthy control (HC), ankylosing spondylitis model (AS), moxibustion at acupuncture points (MA) and moxibustion at non-acupuncture points (MNA) groups (n=8 mice per group). ##p < 0.01: AI score was significant increased at 20 week in the AS, MA and MNA group when compared with the HC group; *p < 0.05: AS vs. MA. The serum levels of serum levels of CRP (B), IFN-γ (C), IL-17 (D), ALP (E) and OCN (F) were determined by ELISA test. Data are expressed as means ± standard deviation from the HC, AS, MA, and MNA group. ##p < 0.01: HC vs. AS, **p < 0.01: AS vs. MA, a: p < 0.05: MA vs. MNA

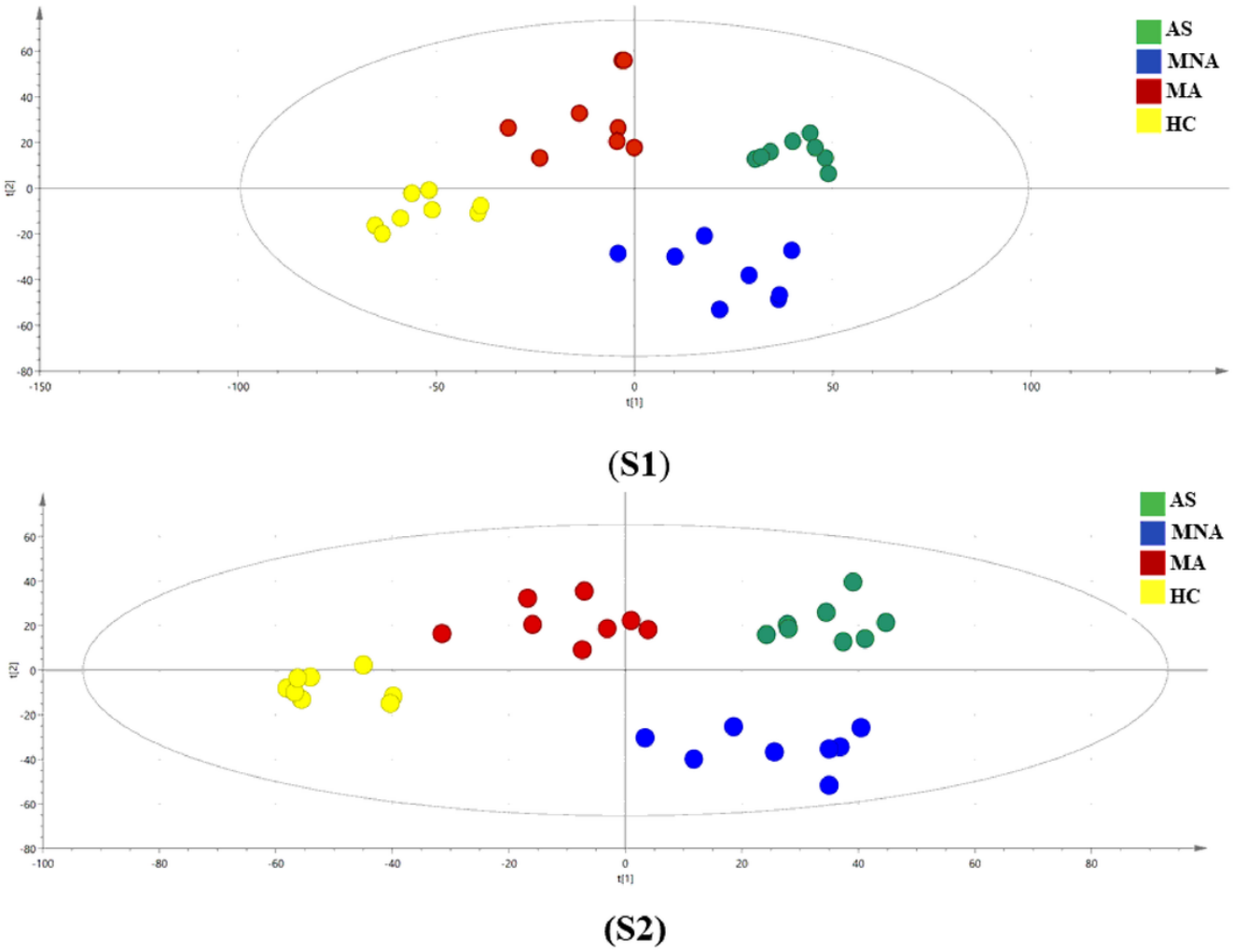

Figure 3

PLS-DA score plots of serum samples (S) from healthy control (HC), ankylosing spondylitis model (AS), moxibustion at acupuncture points (MA) and moxibustion at non-acupuncture points (MNA) in positive and negative ion modes. The label of S1 were obtained in positive ion mode, with the label of S2 in negative ion mode.

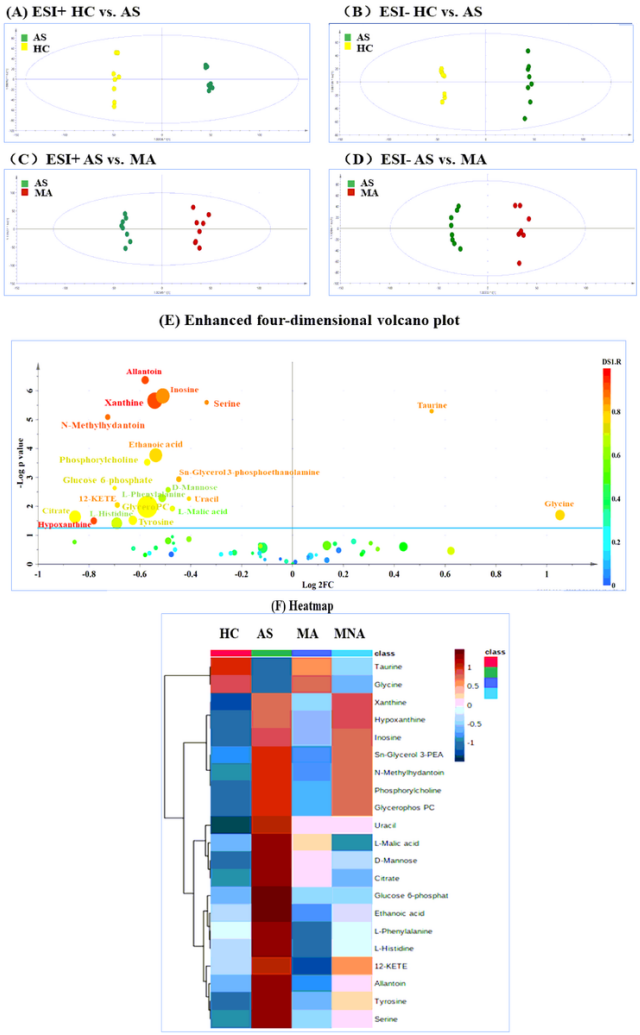

Figure 4

OPLS-DA score plots based on detected serum metabolites from the healthy control (HC) and the ankylosing spondylitis model (AS) in (A) ESI+ mode and (B) ESI- mode. OPLS-DA score plots based on detected serum metabolites from the ankylosing spondylitis model (AS) and the moxibustion at acupuncture points (MA) in (C) ESI+ mode and (D) ESI- mode. (E) The enhanced four-dimensional volcano plot for screening of candidate metabolites. VIP values and correlation coefficient (|r|) values are represented by circles size and color, respectively. A larger circle size corresponds to larger VIP value and warmer color corresponds to higher correlation coefficient |r|. A cut-off blue line represents the threshold (p value=0.05). After log transformation, p<0.05 will have the value of −log (p-value)>1.33. (F) The clustering heatmap is used to provide an intuitive visualization of selecting candidate metabolites. Color differences exhibit the metabolite alteration occur in different groups. (Brown: up-regulation, Blue: down-regulation).

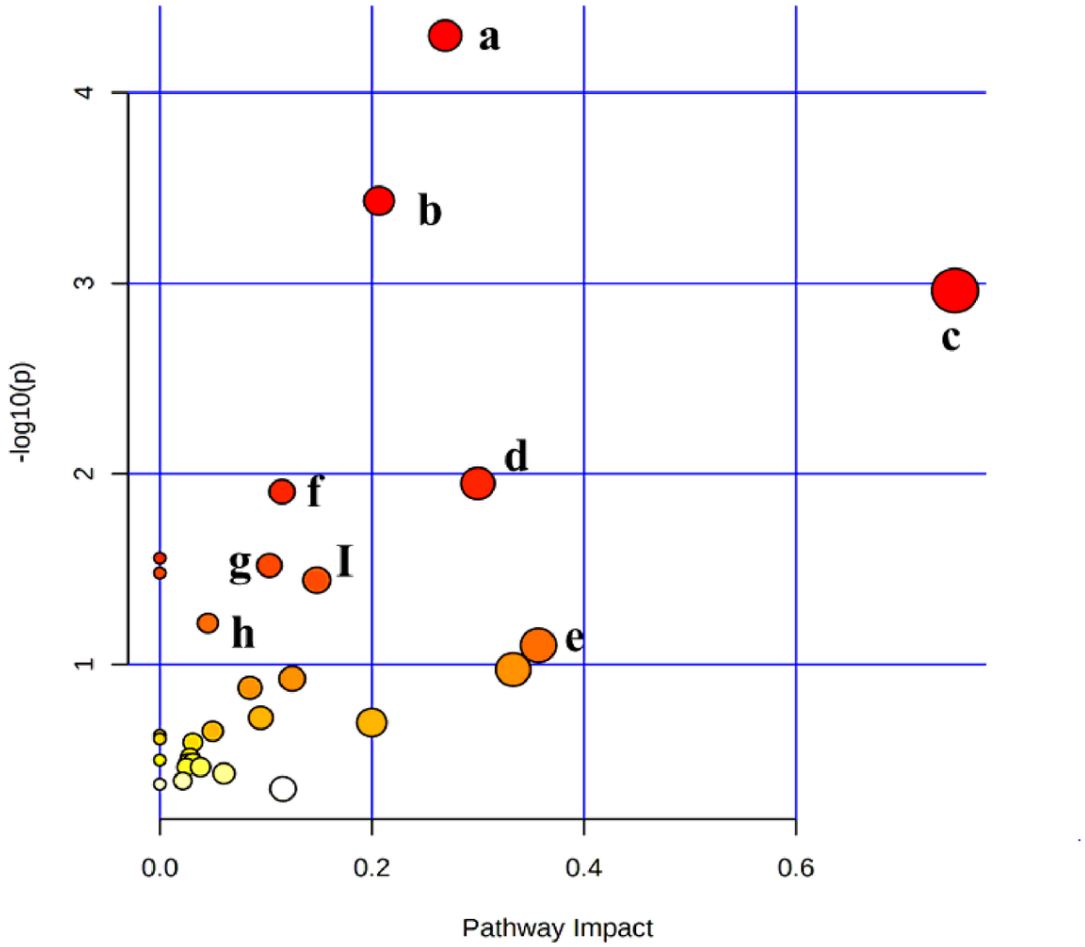

Figure 5

Pathway analysis of significant metabolites. a: Glyoxylate and dicarboxylate metabolism; b: Aminoacyl-tRNA biosynthesis; c: Phenylalanine, tyrosine and tryptophan biosynthesis; d: Phenylalanine metabolism; e: Glycine, serine and threonine metabolism; f: Glycerophospholipid metabolism; g: Citrate cycle (TCA cycle); h: Purine metabolism and i: Pyruvate metabolism.

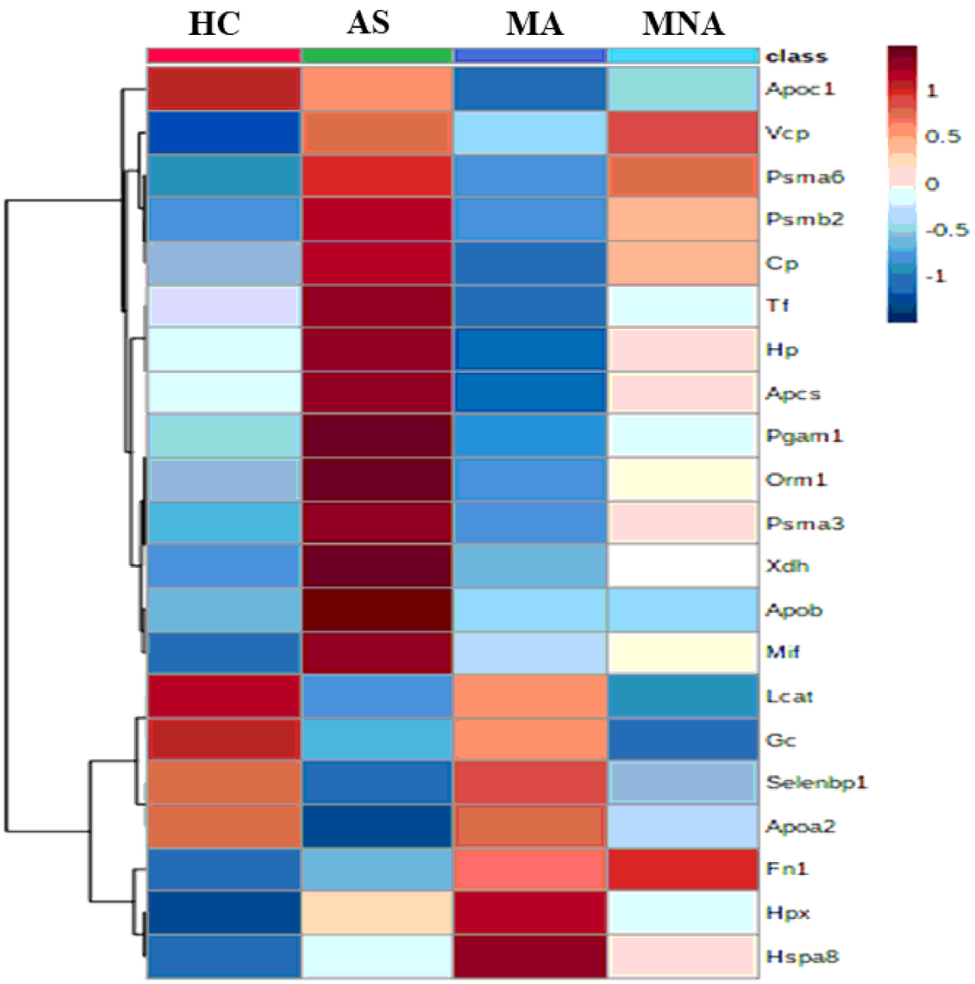

Figure 6

Heatmaps visualization of the 21 differentially abundant proteins.

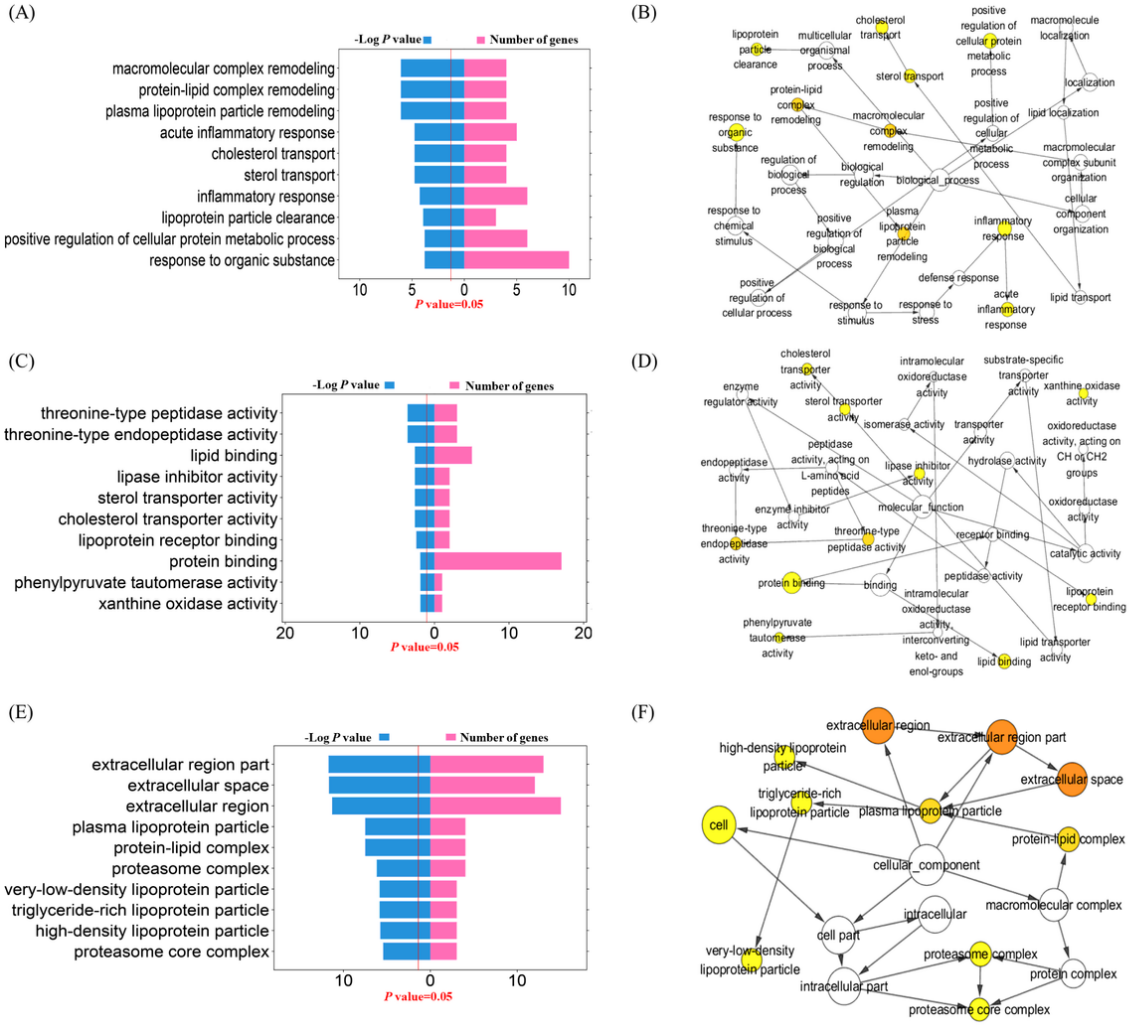

Figure 7

Graph of the top 10 significant pathways of biological function category (A), molecular function category (C), and subcellular localization category (E). The blue color frame indicates the statistical differences of the GO terms via adjust P-value using Benjamini–Hochberg method. A cut-off red line represents the threshold (adjust p value=0.05). After log transformation, p<0.05 will have the value of −log (p-value)>1.33. The pink color frame represents the number of proteins. Enrichment analysis of the biological function category (B), molecular function category (D), and subcellular localization category (F); each node means one different biological function, molecular function, or subcellular localization and more significant ones are filled in with a deeper color.

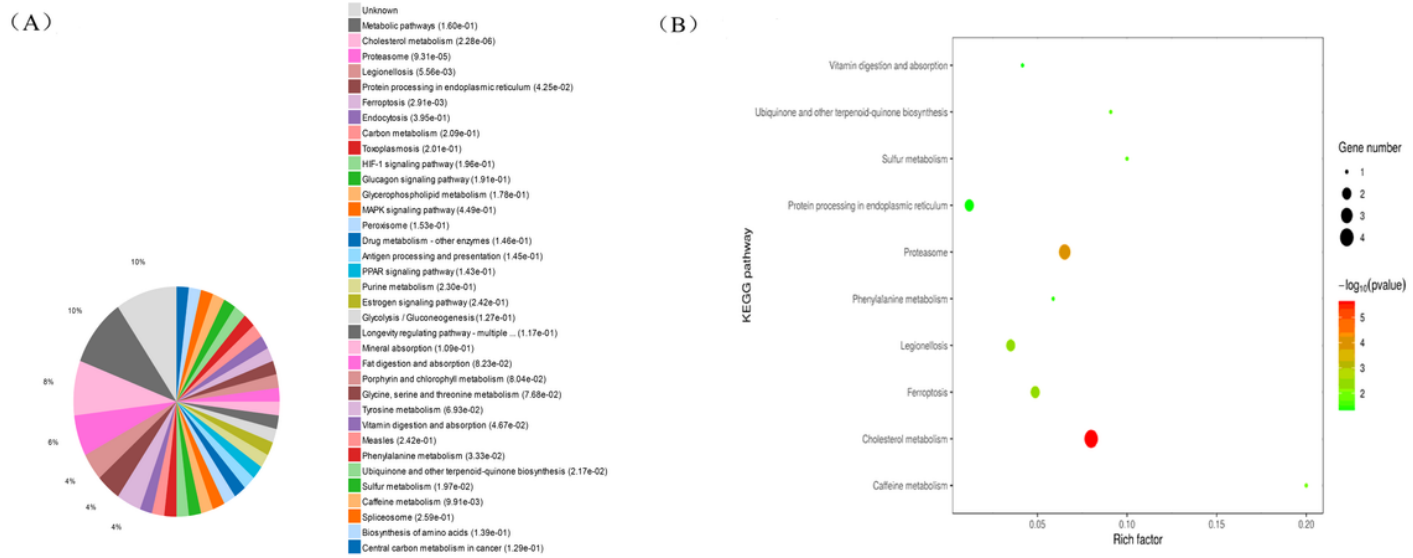

Figure 8

(A) KEGG classification of the identified proteins in serum samples using the Omicbean classification system (http://www.omicsbean.cn/). (B) Bubble plot of the top 10 most significant associated KEGG pathways.

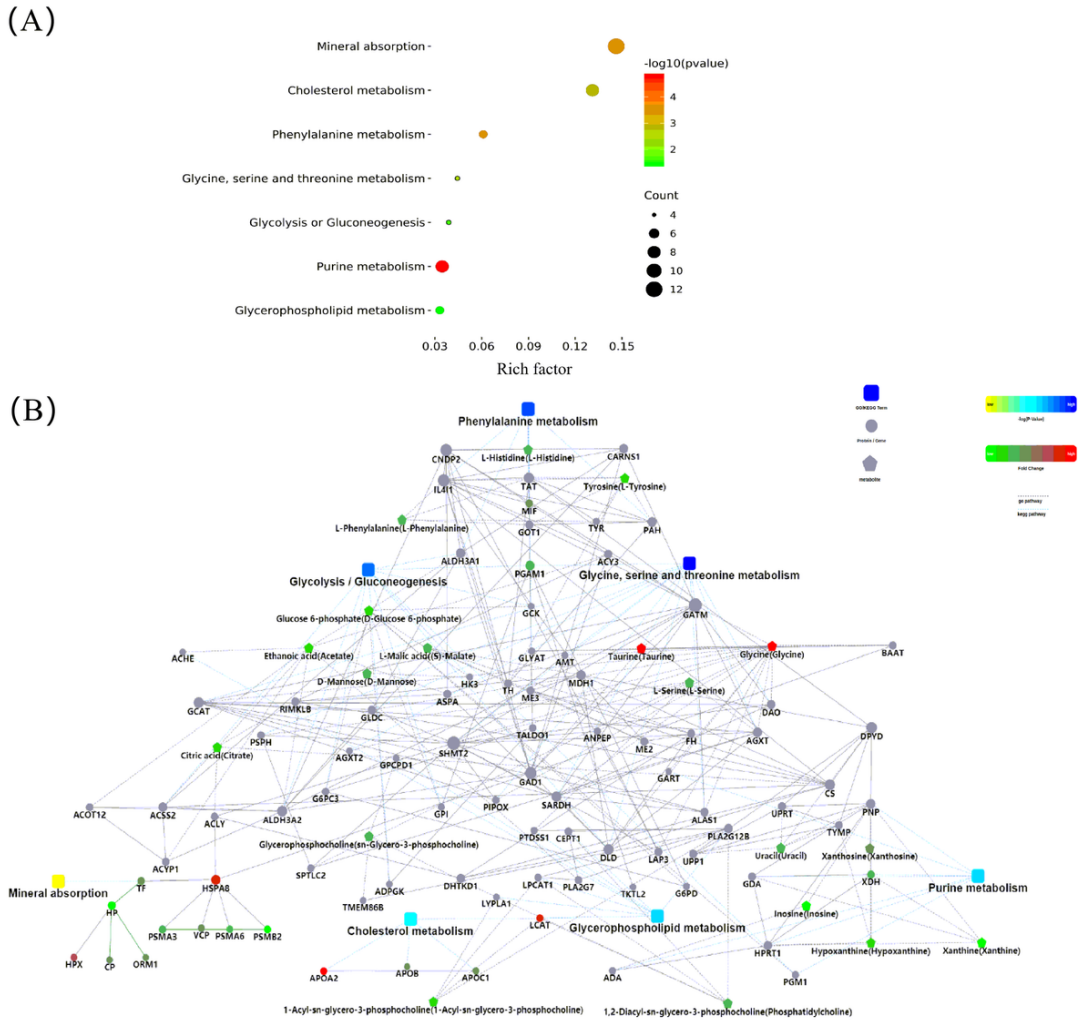

Figure 9

(A) The 7 canonical pathways categories of the differential metabolites and proteins affected. (B) Protein–metabolite interaction analysis by the OmicsBean.

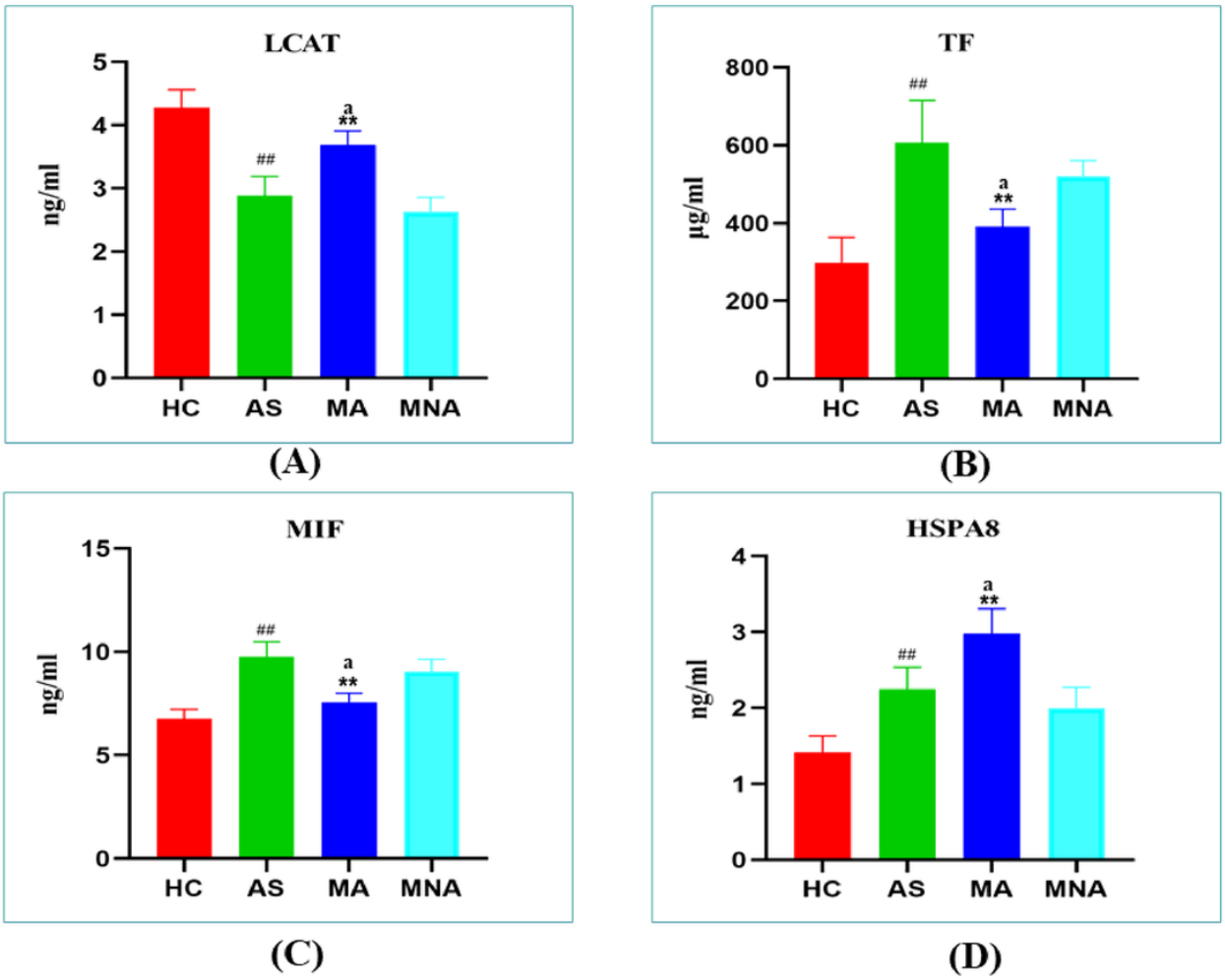

Figure 10

The serum levels of serum levels of LCAT (A), TF (B), MIF (C), and HSPA8 (D) were determined by ELISA test. Data are expressed as means ± standard deviation from the HC, AS, MA, and MNA group. ##p < 0.01: HC vs. AS, **p < 0.01: AS vs. MA, a: p < 0.05: MA vs. MNA

Supplementary Files

This is a list of supplementary files associated with this preprint. Click to download.

- renamed00e3e.pdf